Biogeosciences

Influence of atmospheric deposition on biogeochemical cycles in an oligotrophic ocean system

France Van Wambeke[1], Vincent Taillandier[2], Karine Desboeufs[3], Elvira Pulido-Villena[1], Julie Dinasquet[4,5], Anja Engel[6], Emilio Marañón[7], Céline Ridame[8], and Cécile Guieu[2]

[1]Mediterranean Institute of Oceanography (MIO), UM 110, Aix-Marseille Université, CNRS, INSU,
Université de Toulon, IRD, 13288 Marseille, France
[2]Laboratoire d'Océanographie de Villefranche (LOV), UMR 7093, CNRS, Sorbonne Université,
06230 Villefranche-sur-Mer, France
[3]Université de Paris and Univ Paris-Est Créteil, CNRS, LISA, 75013 Paris, France
[4]Laboratoire d'Océanographie Microbienne (LOMIC), Observatoire Océanologique, Sorbonne Université,
66650 Banyuls-sur-Mer, France
[5]Marine Biology Research Division, Scripps Institution of Oceanography, UCSD, La Jolla, CA, USA
[6]GEOMAR – Helmholtz Centre for Ocean Research, Kiel, Germany
[7]Department of Ecology and Animal Biology, Universidade de Vigo, 36310 Vigo, Spain
[8]Laboratoire d'Océanographie et du Climat: Expérimentation et Approches Numériques (LOCEAN), UMR 7159,
Sorbonne Université, CNRS, IRD, MNHN, 4 Place Jussieu, 75252 Paris CEDEX 05, France

Correspondence: France Van Wambeke (france.van-wambeke@mio.osupytheas.fr) and Cécile Guieu (guieu@imev-mer.fr)

Abstract. The surface mixed layer (ML) in the Mediterranean Sea is a well-stratified domain characterized by low macronutrients and low chlorophyll content for almost 6 months of the year. In this study we characterize the biogeochemical cycling of nitrogen (N) in the ML by analyzing simultaneous in situ measurements of atmospheric deposition, nutrients in seawater, hydrological conditions, primary production, heterotrophic prokaryotic production, N_2 fixation and leucine aminopeptidase activity. Dry deposition was continuously measured across the central and western open Mediterranean Sea, and two wet deposition events were sampled, one in the Ionian Sea and one in the Algerian Basin. Along the transect, N budgets were computed to compare the sources and sinks of N in the mixed layer. In situ leucine aminopeptidase activity made up 14 % to 66 % of the heterotrophic prokaryotic N demand, and the N_2 fixation rate represented 1 % to 4.5 % of the phytoplankton N demand. Dry atmospheric deposition of inorganic nitrogen, estimated from dry deposition of nitrate and ammonium in aerosols, was higher than the N_2 fixation rates in the ML (on average 4.8-fold). The dry atmospheric input of inorganic N represented a highly variable proportion of biological N demand in the ML among the stations, 10 %–82 % for heterotrophic prokaryotes and 1 %–30 % for phytoplankton. As some sites were visited on several days, the evolution of biogeochemical properties in the ML and within the nutrient-depleted layers could be followed. At the Algerian Basin site, the biogeochemical consequences of a wet dust deposition event were monitored through high-frequency sampling. Notably, just after the rain, nitrate was higher in the ML than in the nutrient-depleted layer below. Estimates of nutrient transfer from the ML into the nutrient-depleted layer could explain up to a third of the nitrate loss from the ML. Phytoplankton did not benefit directly from the atmospheric inputs into the ML, probably due to high competition with heterotrophic prokaryotes, also limited by N and phosphorus (P) availability at the time of this study. Primary producers decreased their production after the rain but recovered their initial state of activity after a 2 d lag in the vicinity of the deep chlorophyll maximum layer.

1 Introduction

The Mediterranean Sea (MS) is a semi-enclosed basin characterized by active ventilation and short residence times of the newly formed waters, due to its own thermohaline circulation (MERMEX Group, 2011). In terms of biogeochemistry, the MS is characterized by a long summer stratification period, a west-to-east gradient of increasing oligotrophy and a deficit in phosphorus (P) compared to nitrogen (N) (MERMEX Group, 2011). The last feature is confirmed by a deep N/P ratio for inorganic nutrients, higher than the Redfield ratio, that increases toward the east (Krom et al., 2004).

The relationship between photoautotrophic unicellular organisms and heterotrophic prokaryotes (competition or commensalism) is affected by the balance of light and nutrients as well as possible inputs of organic matter from river runoff or atmospheric deposition. Phytoplankton generally experience P or N limitation or both (Thingstad et al., 2005; Tanaka et al., 2011; Richon et al., 2018), whereas heterotrophic prokaryotes are usually P limited or P and organic carbon co-limited (Sala et al., 2002; Van Wambeke et al., 2002; Céa et al., 2014).

The MS continuously receives anthropogenic aerosols, originating from industrial and domestic activities around the basin and from other parts of Europe, along with pulsed natural inputs from the Sahara. It is thus a natural low-nutrient–low-chlorophyll (LNLC) study area, well adapted to investigating the role of ocean–atmosphere exchanges of particles and gases on marine biogeochemical cycles. Recent studies describe annual records of atmospheric deposition of trace metals and inorganic macronutrients (N, P) obtained at several locations around the MS (Markaki et al., 2010; Guieu and Ridame, 2021; Desboeufs, 2021). All records show pulsed and highly variable atmospheric inputs. Recent models and observations show that atmospheric deposition of organic matter (OM) is also highly variable and that its annual inputs are of the same order of magnitude as river inputs (Djaoudi et al., 2017; Kanakidou et al., 2018, 2020; Galetti et al., 2020). Moreover, the sum of atmospheric inputs of nitrate, ammonium and soluble organic nitrogen has been shown to be equivalent to or higher than those from N_2 fixation (Sandroni et al., 2007). In addition inorganic atmospheric N inputs alone may also be higher than N_2 fixation rates (Bonnet et al., 2011).

Aerosol amendments in bottles, minicosms or mesocosms have been widely used to study trophic transfer and potential export, as they allow natural communities to be studied under controlled conditions (i.e., Guieu et al., 2010; Herut et al., 2016; Mescioglu et al., 2019). Both the diversity and the functioning of various biological compartments are impacted by aerosol additions in different waters tested in the MS (Guieu and Ridame, 2021, and Fig. 3 therein). Differences in the biological responses have been observed, depending on the mode of deposition simulated (wet or dry), the type of aerosols used (natural or anthropogenic) and the

in situ biogeochemical conditions at the time of the experiment (Guieu and Ridame, 2021).

A fraction of organic carbon from aerosols is soluble, and this soluble fraction is partly available to marine heterotrophic prokaryotes (Djaoudi et al., 2020). Heterotrophic prokaryotes have the metabolic capacity to respond quickly to aerosol deposition through growth and changes in community composition (Rahav et al., 2016; Pulido-Villena et al., 2008, 2014), while the phytoplankton community responds more slowly or not at all (Guieu and Ridame, 2021, and references therein).

Owing to the intrinsic limitations of experiments in enclosures, which vary depending on the volume and design (i.e., the omission of higher trophic levels, absence of turbulent mixing limiting exchanges by diffusion and wall effects), such experiments cannot fully simulate in situ conditions (Guieu and Ridame, 2021). Thus, in situ observations are required to understand the consequences of aerosol deposition for biogeochemical cycling in the world's ocean. Such in situ studies are scarce and require dedicated, high-frequency sampling to follow the effects of deposition on the biogeochemical processes while taking into account the water column dynamics as recently emphasized in cases studies (Pulido-Villena et al., 2008; Rahav et al., 2016).

Hence, there is a need for sampling surveys with adaptive strategies to follow aerosol deposition events in situ and their impacts on biogeochemical processes, especially in the open waters of the stratified and nutrient-limited MS. The objectives of the PEACETIME project were to study fundamental processes and their interactions at the ocean–atmosphere interface following atmospheric deposition (especially of Saharan dust) in the Mediterranean Sea and how these processes impact the functioning of the pelagic ecosystem (Guieu et al., 2020).

As atmospheric deposition affects primarily the surface mixed layer (ML), the present study focuses on the upper part of the nutrient-depleted layer that extends down to the nutriclines (as defined by Du et al., 2017). During the stratification period, concentrations of nitrate and phosphate inside the ML are often below the detection limits of standard methods. However, nanomolar concentrations of nitrate (and phosphate) can now be assessed accurately through a long waveguide capillary cell (LWCC) technique (Zhang and Chi, 2002), which permits the measurement of fine gradients inside nutrient-depleted layers of the MS (Djaoudi et al., 2018).

The aims of the present study were to assess the impact of atmospheric nutrient deposition on biogeochemical processes and fluxes in the open sea during the PEACETIME cruise in the MS. For this (i) we estimated nanomolar variations in nitrate concentration in the surface mixed layer (ML) under variable inputs of dry and wet aerosol deposition and (ii) we compared the aerosol-derived N inputs to the ML with biological activities: primary production, heterotrophic prokaryotic production, N_2 fixation and ectoenzymatic (leucine aminopeptidase) activity. We studied the N

budgets along a zonal transect that includes 13 stations crossing the Algerian Basin, Tyrrhenian Sea and Ionian Sea where dry atmospheric deposition was continuously measured on board together with biogeochemical, biological and physical seawater characteristics. We finally focused on a wet deposition event that occurred in the western Algerian Basin, where we investigated the evolution of biogeochemical fluxes of both N and P and microbial activities through high-frequency sampling.

2 Materials and methods

2.1 Sampling strategy and measured parameters

The PEACETIME cruise (https://doi.org/10.17600/15000900) was conducted in the Mediterranean Sea, from May to June 2017, along a transect extending from the western basin to the center of the Ionian Sea (Fig. 1). For details on the cruise strategy, see Guieu et al. (2020). Short-duration stations (<8 h, 10 stations named ST1 to ST10, Fig. 1, also referred to as "short stations" in the text) and long-duration sites (5 d, 3 sites named TYR, ION and FAST) were occupied. Chemical composition of aerosols was quantified by continuous sampling along the whole transect. In addition, two rain events were sampled (Desboeufs et al., 2021.), one on 29 May at ION and a second one, a wet dust deposition event, at FAST on 5 June.

At least three CTD casts were conducted at each short station. One cast focused on the epipelagic layer (0–250 m) and another on the whole water column. Two casts were carried out with a standard CTD rosette equipped with 24 Niskin bottles (12 L) and a Sea-Bird SBE 9 underwater unit with pressure, temperature (SBE 3), conductivity (SBE 4), chlorophyll fluorescence (Chelsea Acquatracka) and oxygen (SBE 43) sensors. A third cast, from the surface to the bottom of the water column, was carried out under trace metal clean conditions using an instrumental package including a titanium rosette (hereafter TMC rosette) mounted on a Kevlar cable and equipped with Go-Flo bottles that were sampled in a dedicated clean lab container. The long-duration sites were abbreviated as TYR (situated in the center of the Tyrrhenian Basin), ION (in the center of the Ionian Basin) and FAST (in the western Algerian Basin). These three sites were selected based on satellite imagery, altimetry and Lagrangian diagnostics as well as forecasted rain events (Guieu et al., 2020). At these sites, repeated casts were performed over at least 4 d with alternating CTD and TMC rosettes (Table 1). The succession of CTD casts at the FAST site is numbered in days relative to a rain event sampled on board the ship. The first cast of the series was sampled 2.3 d before the rain event and the last 2 d after. The FAST site was revisited following the study at ST10 (3.8 d after the rain event).

Primary production (PP), prokaryotic heterotrophic production (BP), heterotrophic prokaryotic abundances (hprok),

ectoenzymatic activities (leucine aminopeptidase (LAP) and alkaline phosphatase (AP)), were determined in water samples collected with the standard CTD rosette. Dissolved inorganic nutrients, dissolved organic nitrogen (DON) and dissolved organic phosphorus (DOP) were measured in water samples collected using the TMC rosette. LAP and AP were determined from two layers in the epipelagic waters (5 m depth and deep chlorophyll maximum (DCM)) at the short stations and at the ION and TYR sites. In addition, LAP and AP were determined at four depths between 0 and 20 m for four profiles at the FAST site to determine the variability within the ML.

2.2 Analytical methods and flux calculations

2.2.1 Nutrients in the atmosphere

Total suspended aerosol particles (TSP inlet) were collected continuously throughout the campaign for dry deposition estimations. Aerosol sampling was carried out using filtration units on adapted membranes for off-line chemical analysis (Tovar-Sanchez et al., 2020). Simultaneously, the water-soluble fraction of the aerosols was sampled continuously, using a particle-into-liquid sampler (PILS; Orsini et al., 2003). Moreover, two wet deposition events were sampled, one at ION and one at FAST using rain collectors with on-line filtration (porosity 0.2 µm) (details in Desboeufs et al., 2021).

Nitrate and ammonium concentrations in the aerosols, abbreviated in the text as NO3 and NH4, respectively, were analyzed continuously on board from 13 May, using PILS sampling coupled on-line with double-way ion chromatography (PILS-IC, Metrohm, model 850 Professional IC with Metrosep A Supplement 7 column for anion measurements and Metrosep C4 column for cation measurements). The temporal resolution for PILS-IC analysis was 70 min for anions and 32 min for cations. Dissolved inorganic nitrogen (DIN) fluxes released by dry deposition were estimated by multiplying NO3 and NH4 obtained through PILS-CI measurements (nitrite concentrations were under analytical detection limits) by the dry settling velocities of N-bearing aerosols, i.e., 0.21 and 1 cm s^{-1} for NH4 and NO3, respectively (Kouvarakis et al., 2001). Mean NO3 and NH4 concentrations were calculated from the PILS-IC data measured (1) during the occupation of each short station lasting between 0.13 and 0.66 d (with on average 5 measurements for NO3 and 11 measurements for NH4) and (2) between two successive casts at the sites with a time lag of between 0.4 and 1.21 d (with on average 15 measurements for NO3 and about 30 for NH4). At ST1, NH4 and NO3 concentrations were obtained using IC analyses following water extraction from aerosol filter sampling as the PILS-IC instrument was not operational.

Total dissolved phosphate (TDP) concentrations were estimated from soluble P concentrations extracted from particulate aerosols collected on filters after ultrapure water extrac-
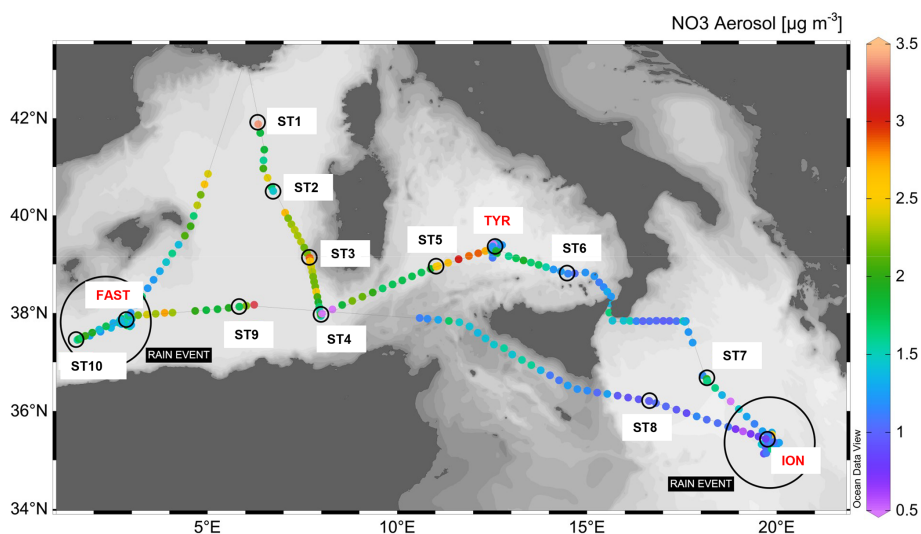
Figure 1. Nitrate (NO3) concentrations in the aerosols along the PEACETIME transect. The locations of two rain events are indicated by large black circles. Stations ST1 to ST4 were not sampled for nutrient analysis at a nanomolar level. Software for figure plot: Schlitzer (2021).

Table 1. Main biogeochemical features/trophic conditions during the PEACETIME cruise. For TYR, ION and FAST sites investigated over several days, means $\pm$ SD are indicated. ITChl a: integrated total chlorophyll a (Chl a + divinyl Chl a); IPP: integrated particulate primary production; IBP: integrated heterotrophic prokaryotic production. Integrations from surface to 200 m depth for all data except IPP, integrated down to the depth of the 1 % photosynthetically active radiation (PAR) level. nd: no data.

	Sampling date	Lat °N	Long °E	Temp at 5 m (°C)	Bottom depth (m)	DCM depth (m)	ITChl a (mg Chl a m^{-2})	IPP (mg C m^{-2} d^{-1})	IBP (mg C m^{-2} d^{-1})
ST1	12 May	41°53.5′	6°20′	15.7	1580	49	35.0	284	51
ST2	13 May	40°30.36′	6°43.78′	17.0	2830	65	32.7	148	55
ST3	14 May	39°8.00′	7°41.0′	14.3	1404	83	23.2	140	77
ST4	15 May	37°59.0′	7°58.6′	19.0	2770	64	29.2	182	66
ST5	16 May	38°57.2′	11°1.4′	19.5	2366	77	30.5	148	51
TYR	17–20 May	39°20.4′	12°35.56′	19.6	3395	80 $\pm$ 6	29 $\pm$ 3	170 $\pm$ 35	57 $\pm$ 3
ST6	22 May	38°48.47′	14°29.97′	20.0	2275	80	18.7	142	62
ST7	24 May	36°39.5′	18°9.3′	20.6	3627	87	24.2	158	57
ION	25–28 May	35°29.1′	19°47.77′	20.6	3054	97 $\pm$ 5	29 $\pm$ 2	208 $\pm$ 15	51 $\pm$ 9
ST8	30 May	36°12.6′	16°37.5′	20.8	3314	94	31.6	206	71
ST9	2 June	38°8.1′	5°50.5′	21.2	2837	91	36.1	214	64
FAST	2–7 and 9 June	37°56.8′	2°54.6′	21.0	2775	79 $\pm$ 8	34 $\pm$ 8	211 $\pm$ 57	92 $\pm$ 11
ST10	8 June	37°27.58′	1°34.0′	21.6	2770	89	28.9	nd	96

tion and high-resolution inductively coupled plasma mass spectrometry (HR-ICP-MS) analysis (Neptune Plus, Thermo Scientific™) since it was generally below the detection limits of the PILS-IC technique. The frequency of TDP analysis was therefore less than for NO3 and NH4 (0.28–1.15 d depending on the stations). At ION, TYR and FAST, filters collected aerosols at different periods including during each CTD cast when possible.

Atmospheric deposition of soluble P was estimated by multiplying the TDP concentration by a dry settling velocity of 1 cm s^{-1}, except at FAST where 3 cm s^{-1} was used as this value is better adapted for lithogenic particles (Izquierdo et al., 2012). The dissolved fraction and solution from digestion

(Heimburger et al., 2012) of particulate fractions in the filters were analyzed by ICP-AES (inductively coupled plasma atomic emission spectrometry, Spectro ARCOS Ametek®). The organic/inorganic speciation of TDP was determined from HR-ICP-MS and IC analysis. DOP was estimated from the difference between TDP, obtained by HR-ICP-MS, and DIP, obtained by ion chromatography.

In the rain samples, NO3, NH4 and dissolved inorganic phosphorus (DIP) were also determined using ion chromatography following recovery of the dissolved fraction. Total particulate P (TPP) and dissolved organic P (DOP) were also measured in the rain samples following the protocol used for atmospheric dust (described above). The wet deposition

fluxes of dissolved nutrients and particulate fractions were estimated from the measured concentrations in the rain sample multiplied by total precipitation.

Total precipitation was taken from the total hourly precipitation accumulated during the rain event over the region from the ERA5 hourly data reanalysis (Hersbach et al., 2018). In order to incorporate the regional variability in rainfall, the total precipitation was taken from the total hourly precipitation over a domain whose center is the ship with a radius of 110 km using the ERA5 hourly data reanalysis (Hersbach et al., 2018). ERA5 data are available on regular latitude–longitude grids at a $0.25° \times 0.25°$ resolution (Desboeufs et al., 2021). Cumulative precipitation (Table 3) was obtained by considering the value at the center of each grid point over the domain.

2.2.2 Nutrients in the water column

Seawater samples for standard nutrient analysis were filtered on-line ($< 0.2\,\mu m$, Sartorius Sartobran P capsule with a $0.45\,\mu m$ prefilter and a $0.2\,\mu m$ final filter) directly from the Go-Flo bottles (TMC rosette). Samples collected in acid-washed polyethylene bottles were immediately analyzed on board. Micromolar concentrations of nitrate + nitrite (NO_x) and DIP were determined using a segmented flow analyzer (AA3 HR Seal Analytical) following Aminot and Kérouel (2007) with a limit of quantification (calculated as 10 times the standard deviation of 10 measurements of the blank) of $0.050\,\mu M$ for NO_x and $0.020\,\mu M$ for DIP. Samples for the determination of nanomolar concentrations of dissolved nutrients were collected in HDPE bottles previously cleaned with supra-pure HCl. For NO_x (primarily NO3 as the nitrite fraction was mostly negligible), samples were acidified to a pH of 1 inside the clean container and analyzed back in the home laboratory using spectrophotometry at 540 nm, with a 1 m LWCC (Louis et al., 2015). The detection limit was 6 nM; the limit of quantification was 9 nM, and the reproducibility was 8.5 %. DIP was analyzed immediately after sampling using the LWCC method after Pulido-Villena et al. (2010), with a detection limit of 1 nM (Pulido-Villena et al., 2021). Total dissolved phosphorus (TDP) and total dissolved nitrogen (TDN) were measured using the segmented flow analyzer technique after high-temperature (120 °C) persulfate wet oxidation mineralization (Pujo-Pay and Raimbault, 1994). DON was obtained as the difference between TDN and NO_x. DOP was obtained as the difference between TDP and DIP. Labile DOP (L-DOP) was estimated as 31 % of the DOP values (Pulido-Villena et al., 2021).

Total hydrolysable amino acids (TAAs) were determined as described in detail by Van Wambeke et al. (2021). Briefly, 1 mL of sample was hydrolyzed at 100 °C for 20 h with 1 mL of 30 % HCl and then neutralized by acid evaporation. Samples were analyzed by high-performance liquid chromatography in duplicate according to Dittmar et al. (2009) protocols.

2.2.3 Biological stocks and fluxes in the epipelagic waters

Flow cytometry was used for the enumeration of autotrophic prokaryotic and eukaryotic cells, heterotrophic prokaryotes (hprok), and heterotrophic nanoflagellates (HNF). Water samples (4.5 mL) were fixed with glutaraldehyde grade-I 25 % (1 % final concentration), flash frozen and stored at −80 °C until analysis. Counts were performed on a FAC-SCanto II flow cytometer (Becton, Dickinson and Company). The separation of different autotrophic populations was based on their scattering and fluorescence signals according to Marie et al. (2000). For the enumeration of hprok (Gasol and Del Giorgio, 2000), cells were stained with SYBR Green I (Invitrogen – Molecular Probes). HNF staining was performed with SYBR Green I as described in Christaki et al. (2011). All cell abundances were determined from the flow rate, which was calibrated with TruCount beads (BD Biosciences).

Primary production (PP) was determined at six layers from the shallow CTD casts (0–250 m) sampled before sunrise. Samples were inoculated with ^{14}C bicarbonate and incubated in on-deck incubators kept at in situ temperature by flowing surface seawater and equipped with various blue screens to simulate different irradiance levels. After 24 h incubations, samples were filtered through $0.2\,\mu m$ polycarbonate filters and treated for liquid scintillation measurement as described in detail in Marañón et al. (2021). A temperature correction was applied as explained in Marañón et al. (2021). N_2 fixation rates (N2fix) were determined as described in Ridame et al. (2011) using 2.3 L of unfiltered seawater collected in acid-washed polycarbonate bottles and enriched with $^{15}N_2$ gas (99 at. % ^{15}N) to obtain a final enrichment of about 10 at. % excess. For N2fix, 24 h incubations were conducted under the same temperature and irradiance as the corresponding PP incubations.

To calculate heterotrophic prokaryotic production (BP), samples collected in the epipelagic layers (0–250 m) were incubated with tritiated leucine using the microcentrifuge technique as detailed in Van Wambeke et al. (2021). We used the empirical conversion factor of 1.5 ng C per picomole of incorporated leucine according to Kirchman (1993). Isotope dilution was negligible under these saturating concentrations as periodically checked with concentration kinetics. As we used only two onboard temperature-controlled dark incubators, a temperature correction was applied as explained in Van Wambeke et al. (2021). Ectoenzymatic activities were measured fluorometrically, using the fluorogenic model substrates L-leucine-7-amido-4-methylcoumarin (Leu-MCA) and 4-methylumbelliferyl phosphate (MUF-P) to track aminopeptidase (LAP) and alkaline phosphatase (AP) activity, respectively, as described in Van Wambeke et al. (2021). Briefly, the release of MCA from Leu-MCA and MUF from MUF-P was followed by measuring the increase in fluorescence in the dark (excitation

and emission 380 and 440 nm for MCA and 365 and 450 nm for MUF, wavelength width 5 nm) in a Varioskan LUX microplate reader. Fluorogenic substrates were added at varying concentrations (0.025, 0.05, 0.1, 0.25, 0.5 and 1 μM) in 2 mL wells in duplicate. The parameters V_m (maximum hydrolysis velocity) and K_m (Michaelis–Menten constant that reflects enzyme affinity for the substrate) as well as their corresponding errors were estimated by non-linear regression using the Michaelis–Menten equation:

$$V = V_m \times S/(K_m + S), \tag{1}$$

where V is the hydrolysis rate and S the fluorogenic substrate concentration added. We used an approach similar to that of Hoppe et al. (1993) to compute the in situ hydrolysis rates for LAP and AP. We assumed that total amino acids (TAAs) could be representative of dissolved proteins. LAP and AP in situ activities were thus determined by substituting S with TAA and L-DOP in situ concentrations, respectively, in the Michaelis–Menten equations (Van Wambeke et al., 2021; Pulido-Villena et al., 2021).

2.3 Vertical nutrient fluxes

In the absence of concomitant turbulence measurements, the mixed layer depth (MLD) can be estimated from density profiles (e.g., de Boyer Montegut et al., 2004; D'Ortenzio et al., 2005). For this study, a MLD was determined at every CTD cast as the depth where the residual mass content (i.e., the vertical integral of the density anomaly relative to the surface) was equal to 1 kg m^{-2} (Prieur et al., 2020), with an error of estimation of 0.5 m relative to the vertical resolution of the profile (1 m).

In the Mediterranean Sea, the low nutrient availability combined with a shallow mixed layer (ML) led to the formation of a nutrient-depleted layer that extended below the ML. Hereafter, the nutrient-depleted layer is referred to as the "NDLb" (b for bottom or base) for NO3 and as PDLb for DIP (Fig. 2). The base of both layers corresponds to the nitracline and phosphacline depths, respectively, estimated by the deepest isopycnal at which measurements of NO3 and DIP, respectively, reach the detection limit (Kamykowski and Zentara, 1985; Omand and Mahadevan, 2015). Both the nitracline depth and the phosphacline depth are estimated at every discrete profile from the intercept of the regression line reported in a nutrient–density diagram.

Exchanges of nutrients between the ML and NDLb or PDLb are driven by diffusion or advection (Du et al., 2017). The flux of nutrients is a one-dimensional setting and can be expressed as

$$F_{NO3} = F_{DIF} + F_{ADV}. \tag{2}$$

The diffusive flux F_{DIF} is expressed as the gradient of nutrient concentration times a vertical diffusivity coefficient K_z:

$$F_{DIF} = K_z \times (NO3_{ML} - NO3_{NDLb}) \div MLD. \tag{3}$$
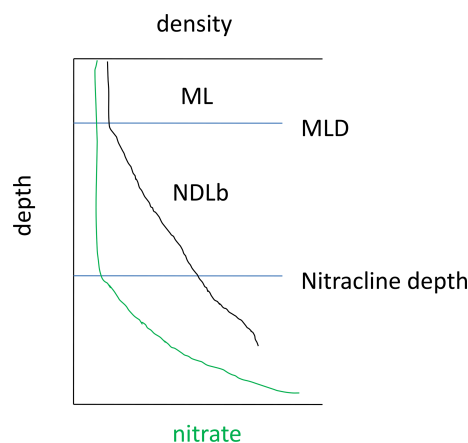
Figure 2. Diagram showing the mixed layer (ML) and the bottom of the nitrate (NO3)-depleted layer (NDLb), delineated by the nitracline depth and the mixed layer depth (MLD) as defined in this study.

The typical magnitude of K_z in the surface layers of the PEACETIME stations was assessed to be 10^{-5} m^2 s^{-1}, as discussed in Taillandier et al. (2020).

The advective flux F_{ADV} is driven by the entrainment of deeper water in the mixed layer due to the erosion of the near-surface pycnocline, conversely to the detrainment of waters below the mixed layer by restratification, dependent on wind stress and heat flux (Cullen et al., 2002). It is expressed as the variation in the nutrient concentration across the ML times the temporal variation in the MLD, as

$$F_{ADV} = (NO3_{ML} - NO3_{NDLb}) \times dMLD \div dt. \tag{4}$$

Shallow MLs such as the ones observed in this study (10–20 m) are primarily influenced by wind bursts that can lead to intermittent variations in the MLD, of up to several meters per day (10^{-5} m s^{-1}). The resulting advective fluxes provide transient exchanges that are 1 order of magnitude greater than well-established diffusive fluxes. Over the timescale of significant atmospheric deposition events, associated rapid variations in the MLD would promote the input of atmospheric nutrients to be exported below the ML by advection rather than by diffusion. In other terms, using the hypothesis of non-stationary regimes due to rapid changes in atmospheric conditions (that control both the mixing state of the ML and atmospheric nutrient inputs), we assume that vertical advection is the main process of exchange.

At short stations, only single casts were carried out, preventing any estimation of temporal variations in the MLD (dMLD / dt) required for the calculation of vertical advective fluxes. Thus only a qualitative assessment of nutrient fluxes across the ML is given. Vertical distributions of DIP, along the longitudinal transect, are described in detail in a companion paper (Pulido-Villena et al., 2021).
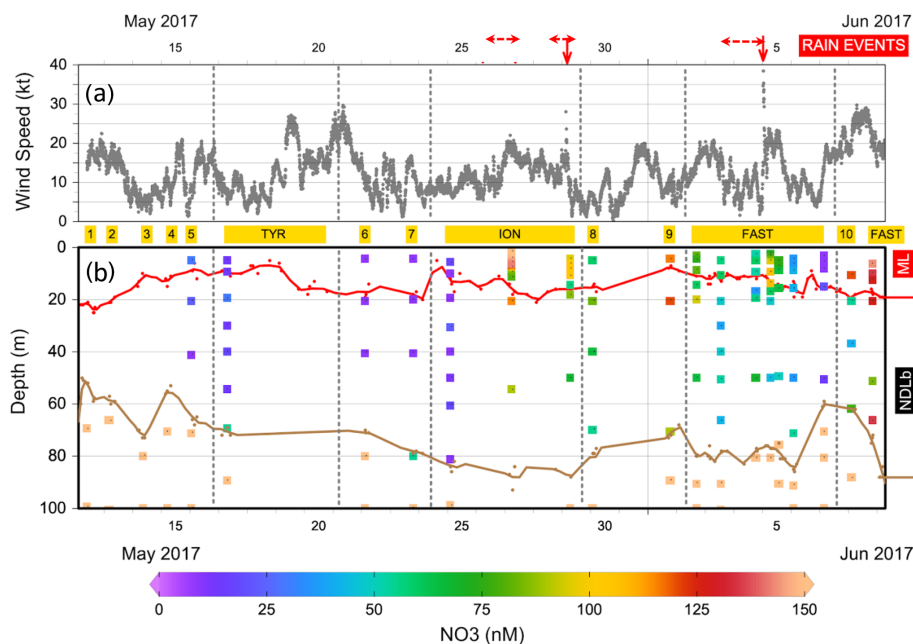
Figure 3. (a) Evolution of the wind speed during the PEACETIME cruise. The stations are indicated in yellow and dates in black. Vertical dashed lines delineate the beginning and the end of the ship's deployment at TYR, ION and FAST. The two rain events collected on board are indicated by the solid vertical red arrows and surrounding observed rain events by horizontal dashed red arrows. **(b)** Distribution of nitrate (NO_3) in the upper 100 m of the water column. The MLD (in red) and nitracline (in brown) are indicated.

2.4 Budget from the metabolic fluxes

Trapezoidal integration was used to integrate BP, PP and N2fix within the ML. The biological activity at the surface was considered to be equal to that of the first layer sampled (around a 5 m depth at the short stations and 1 m depth at FAST). When the base of the ML was not sampled, the values at that depth were estimated through linear interpolation between the two closest data points above and below the MLD.

For LAP, in situ rates expressed in nanomoles of TAA hydrolyzed per liter per hour were transformed into nitrogen units using N per mole of TAA, as the molar distributions of TAAs were available. Integrated in situ LAP hydrolysis rates were calculated assuming the Michaelis–Menten parameters V_m and K_m obtained at a 5 m depth to be representative of the whole ML. Thus an average in situ volumetric LAP flux in the ML was obtained by combining the average TAA concentrations in the ML with these kinetic parameters and multiplying this volumetric rate by the MLD. Daily integrated BP, AP and LAP activities were calculated from hourly rates ×24. Assuming no direct excretion of nitrogen or phosphorus, the C/N and C/P ratios of cell demand are equivalent to the cellular ratios. We used molar C/N ratios derived from Moreno and Martiny (2018) (range 6–8, mean 7) for phytoplankton and from Nagata et al. (1986) for heterotrophic prokaryotes (range 6.2–8.4, mean 7.3). The C/P ratios of cyanobacteria and picophytoeukaryotes in P-depleted conditions ranged from 107 to 161 (Martiny et al., 2013). Based on

these we used a mean C/P of 130 for phytoplankton. A C/P value of 100 was used for heterotrophic prokaryotes (Godwin and Cotner, 2015).

3 Results

3.1 Nutrient patterns and biological fluxes along the PEACETIME transect

During our study, MLD ranged between 7 m (at ST9) and 21 m (at ST1, Table S1 in the Supplement, Fig. 3). The nitracline was shallow in the Provençal Basin (50–60 m) and 70 m in the eastern Algerian Basin and Tyrrhenian Sea, further deepening in the western Algerian Basin and Ionian Sea (80–90 m, Table S1). Mean NO_3 concentrations in the NDLb ranged from the quantification limit (9 nM) to 116 nM (Table S1, Fig. 4). In the ML, mean NO_3 concentrations ranged from 9 to 135 nM; stations were grouped according to NO_3 concentrations (Table S1). Weak gradients, and therefore low exchange, between the ML and NDLb characterized stations in groups 1 to 3. Stations in group 4 showed high and moderate NO_3 concentrations within the ML and NDLb, respectively, with a large positive difference (>20 nM) between both layers.

At 5 m depth, V_m for leucine aminopeptidase (LAP) ranged from 0.21 to 0.56 nmol Leu-MCA hydrolyzed per liter per hour and K_m from 0.12 to 1.29 µM. The mean TAA concentrations within the ML ranged from 0.17 to
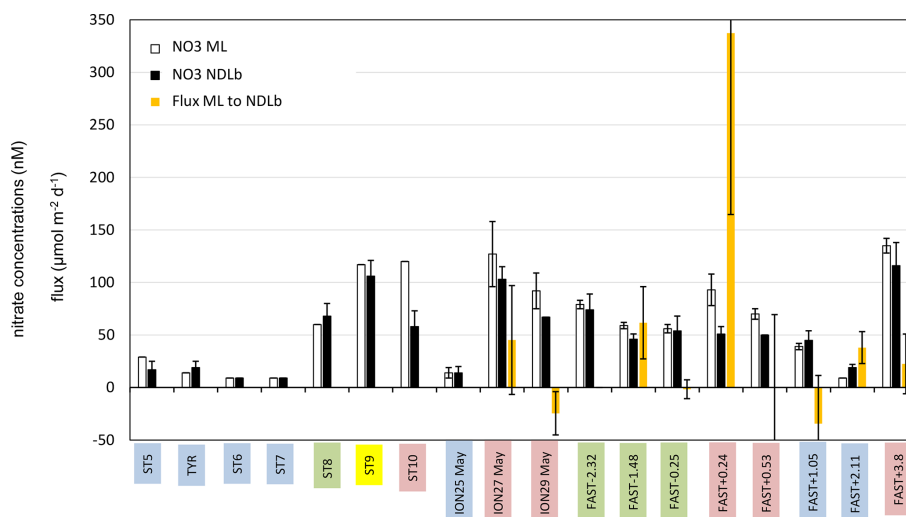
Figure 4. Average concentration of nitrate (NO3) in the ML and NDLb and NO3 flux from the ML into the NDLb. The stations have been classified into four groups (1 in blue, 2 in green, 3 in yellow, 4 in red; see Sect. 3, Results, and Table S1 for definitions). Error bars indicate standard deviation around mean values for nitrate concentrations and error propagation for the flux from the ML to NDLb calculated using a 0.5 m uncertainty in the MLD variation.

0.28 µM. The mean in situ LAP hydrolysis rate within the ML, derived from these parameters, ranged from 0.07 to $0.29\,\mathrm{nmol\,N\,L^{-1}\,h^{-1}}$ (results not shown but detailed in Van Wambeke et al., 2021).

The vertical distributions of PP and BP for the short stations are described in Marañón et al. (2021). Briefly, PP exhibited a deep maximum close to the DCM depth or slightly above, whereas the vertical distribution of BP generally showed two maxima, one within the mixed layer and a second close to the DCM. Integrated PP (Tables 1, S2) ranged from 138 (TYR17 May) to 284 (SD1) $\mathrm{mg\,C\,m^{-2}\,d^{-1}}$. Integrated BP (0–200 m) ranged from 44 (ION27 May) to 113 (FAST + 0.53) $\mathrm{mg\,C\,m^{-2}\,d^{-1}}$. Overall, at the time of the PEACETIME cruise, the transect exhibited the typical west–east gradient of increasing oligotrophy detected by ocean color (see Fig. 8 in Guieu et al., 2020).

3.2   N budgets and fluxes at short stations

Biological rates (all expressed in N units) within the ML at the short stations are shown in Table 2. Phytoplankton N demand (phytoN demand) was the largest, followed by that of heterotrophic prokaryotes (hprokN demand). On average, phytoN demand was 2.9 (range 1.5–8.1) times greater than hprokN demand. LAP hydrolysis rates represented 14 % to 66 % of the hprokN demand (mean ± SD of 37 % ± 19 %) and N_2 fixation rates represented 1 % to 4.5 % of the phytoN demand (2.6 % ± 1.3 %) and 3 % to 11 % of the hprokN demand (6.4 % ± 2.4 %). N_2 fixation rates integrated over the ML correlated slightly better with the hprokN demand ($r = 0.75$) than with the phytoN demand ($r = 0.66$).

Dissolved inorganic N (DIN = NO3 + NH4) solubilized from dry atmospheric deposition ranged from 17 to $40\,\mathrm{\mu mol\,N\,m^{-2}\,d^{-1}}$ with an average contribution of NO3 of 79 % (Table 2). This new DIN input was similar to or higher than N_2 fixation rates within the ML (from 1.3- to 11-fold, mean 4.8-fold). On average, DIN from dry deposition represented 27 % of the hprokN demand (range 10 %–82 %) and 11 % of the phytoN demand (range 1 %–30 %) within the ML.

3.3   Biogeochemical evolution at ION

The ION site was occupied from 25 to 29 May. Rain events in the vicinity of the ship were observed on 26 and 29 May (Desboeufs et al., 2021). On 29 May the rain event was associated with a rain front extending over more than $500\,\mathrm{km^2}$. A rain sample could be taken on board on 29 May between 05:08 and 06:00 (local time), i.e., just 3 h before the last CTD cast. The chemical composition of the rain indicated an anthropogenic origin (Desboeufs et al., 2021).

TDP solubilized from dry atmospheric deposition decreased from $268\,\mathrm{nmol\,P\,m^{-2}\,d^{-1}}$ (25–26 May) to $124\,\mathrm{nmol\,P\,m^{-2}\,d^{-1}}$ (27–28 May). DIN fluxes from dry atmospheric deposition averaged $29 \pm 4\,\mathrm{\mu mol\,N\,m^{-2}\,d^{-1}}$ with small variability during the occupation of the site (Table S2). The molar ratio of DIN/DIP in the rain was 208, and DOP represented 60 % of the total dissolved P (Table 3).

CTD casts were taken every 24 h for biological fluxes or every 48 h for DIP and NO3. Thus the temporal evolution for nutrients in the water column at ION is given only by three profiles. The first profile (25 May before the rain events in the area) made during smooth weather conditions shows a

Table 2. N budget at the short stations within the surface mixed layer (ML): integrated stocks (NO3, μmol N m^{-2}) and fluxes (heterotrophic prokaryotic N demand (hprokN demand), phytoplankton N demand (phytoN demand), in situ leucine aminopeptidase hydrolysis fluxes (LAP), N$_2$ fixation rates (N2fix), and dry atmospheric deposition of NO3 and NH4 (all fluxes in μmol N m^{-2} d^{-1})). Values presented as mean $\pm$ SD. SD was calculated using propagation of errors: for hprokN demand triplicate measurements at each depth and a C/N ratio of 7.3 ± 1.6; for phytoN demand triplicate measurements of PP at each depth and a C/N ratio of 7 ± 1.4; for LAP the analytical TAA error and the V_m and K_m errors; for N2fix the coefficient of variation of 10 % for volumetric fluxes >0.1 nmol N L^{-1} d^{-1} and 20 % for lower values. For dry deposition, SD is based on the variability in the NO3 and NH4 concentrations solubilized from aerosols during the occupation of the station (see "Materials and methods", Sect. 2.2.1). MLD: mixed layer depth. NA: not available because not sampled for LWCC analysis and below detection limits using standard nutrient analysis.

Stations	MLD (m)	Stocks NO3 (μmol N m^{-2})	Biological fluxes phytoN demand (μmol N m^{-2} d^{-1})	hprokN demand (μmol N m^{-2} d^{-1})	LAP (μmol N m^{-2} d^{-1})	N2fix (μmol N m^{-2} d^{-1})	Dry deposition NO3 (μmol N m^{-2} d^{-1})	NH4 (μmol N m^{-2} d^{-1})
ST1	21	NA	1468 ± 325	184 ± 40	121 ± 28	14.6 ± 1.5	18.6 ± 1.4	1.5 ± 0.3
ST2	21	NA	481 ± 161	163 ± 35	48 ± 24	10.7 ± 1.1	23.7 ± 2.2	4.1 ± 0.9
ST3	11	NA	282 ± 82	126 ± 28	40 ± 17	7.8 ± 0.8	33.8 ± 3.6	4.7 ± 0.5
ST4	15	NA	246 ± 80	132 ± 28	83 ± 20	10.7 ± 1.1	23.8 ± 2.9	6.3 ± 2.6
ST5	9	261 ± 22	112 ± 29	42 ± 9	17 ± 12	4.8 ± 0.5	27.0 ± 7.5	7.9 ± 1.8
ST6	18	162 ± 14	410 ± 116	204 ± 44	48 ± 24	9.1 ± 0.9	15.0 ± 0.6	9.3 ± 0.7
ST7	18	162 ± 14	226 ± 123	148 ± 33	83 ± 18	10.5 ± 1.1	23.6 ± 1.9	8.0 ± 1.2
ST8	14	911 ± 77	274 ± 66	130 ± 33	25 ± 8	4.3 ± 0.5	13.4 ± 1.7	3.8 ± 0.6
ST9	7	819 ± 70	259 ± 70	85 ± 22	21 ± 6	3.4 ± 0.4	27.4 ± 3.8	13.5 ± 0.8
ST10	19	2074 ± 176	495 ± 31	294 ± 64	42 ± 26	13.6 ± 1.4	23.9 ± 3.4	4.1 ± 0.4

Table 3. Characteristics and nutrient fluxes estimated in the two rain samples collected during the PEACETIME cruise at ION and FAST.

Event	Rain ION	Rain FAST
Date (day/month) and local time	29/05 05:08–06:00	05/06 02:36–03:04
Estimated precipitation (mm)	3.5 ± 1.2	5.7 ± 1.4
DIP flux (nmol P m^{-2})	663 ± 227	1146 ± 290
DOP flux (nmol P m^{-2})	974 ± 334	908 ± 230
TPP flux (nmol P m^{-2})	239 ± 82	8801 ± 2227
NO3 flux (μmol N m^{-2})	67 ± 22	341 ± 86
NH4 flux (μmol N m^{-2})	71 ± 24	208 ± 53
DIN flux (μmol N m^{-2})	138 ± 47	550 ± 139

shallow ML with low and homogeneous concentrations of NO3 in the ML and the NDLb (Fig. 4). Shortly after, rain events were observed in the area on 26 May although not at the ship's position, and the ML started to deepen 13 h before the second cast sampled for nutrients (on 27 May) and NO3 concentrations increases in the ML and NDLb (Fig. 3). While NO3 concentrations increased in the ML, the effect on the MLD was still moderate as wind conditions rose to 10 m s^{-1} just at the time of the cast (Fig. 3). The interval between the second and the third cast (29 May, cast carried out 3 h after the rain sampled on board) was marked by a slight decrease in wind speed; a deepening of the ML down to 18 m; and a decrease in NO3 in both the ML and the NDLb, with comparatively higher NO3 concentrations in the ML than in the NDLb. The calculation of vertical advective fluxes between the two layers showed a downward flux in the first interval on 25–27 May (Fig. 4, Table S1) and an upward flux in the second interval (27–29 May).

Due to the lack of high-frequency sampling, it was not possible to quantitatively assess the effects of dry/wet atmo-spheric deposition or the effect of nitrate injection from below the NDLd by vertical advection at ION. The intrusion of a low-salinity lens was clearly visible on the thermos-alinograph record and on the 27 May CTD cast, down to a 10 m depth (data not shown). This low-salinity lens could be formed by the rain event noted on 26 May in the vicinity of the station. It was clear that ION on 27 and 29 May was characteristic of group 4 (i.e., higher NO3 concentrations in the ML than in the NDLb), presumably related to NO3 rainfall inputs. The V_m of LAP measured on 25 May at 5 m (0.22 nmol N L^{-1} h^{-1}) was one of the lowest values recorded during the cruise, while the V_m of AP was the highest (5.6 nmol P L^{-1} h^{-1}). PP integrated over the euphotic zone increased slightly from 188 to 226 mg C m^{-2} d^{-1} (Table S2), but due to the variability in the MLD at ION, this trend was not visible when integrating PP over the ML. In the ML, BP increased slightly, from 7.5 to 10.3 mg C m^{-2} d^{-1} between 25 and 29 May, indicating that hprok benefited slightly more from the atmospheric inputs than the autotrophs (Fig. S1, Table S2). The profiles of hprok and *Synechococcus* abundances showed no particular trend with time, with larger variations within the DCM (Fig. S1).

3.4 N budgets and fluxes at FAST

During the occupation of FAST, two rains episodes took place starting on the evening of 2 to 3 June at night and in the early morning of 5 June (Tovar-Sanchez et al., 2020). The radar data indicated the presence of a rain front with patchy, numerous and intense rain events occurring over a large area surrounding the ship's location. These two episodes coincided with a dust plume transported at altitude (between 1 and 4 km) and resulted in wet deposition of dust (Desboeufs

et al., 2021). A rain sample was collected on board on 5 June (between 02:36 and 03:04 LT) and was associated with a wet dust deposition flux of $\sim 40\,\mathrm{mg\,m^{-2}}$. The DIN/DIP ratio in the rain reached 480 (Table 3). After the rain, daily fluxes of DIN solubilized from dry aerosol deposition strongly decreased from 61.2 to $12.9\,\mathrm{\mu mol\,N\,m^{-2}\,d^{-1}}$ between 4 and 5 June.

The water column at the FAST site before the rain event sampled on board ($-2.3, -1.5, -0.25\,\mathrm{d}$) was marked by moderate and similar decreases in NO3 concentrations within the ML and NDLb. Integrated NO3 stocks in the ML (Table S2) reflected slight changes in the MLD (from 14 to 10 m during this time interval). On 5 June, the rain event (Table 3) was associated with a strong wind burst and abrupt mixing. The comparison between NO3 concentrations from two casts, sampled 6 h before and 6 h after the rain (FAST -0.25 and FAST $+0.24$), showed a clear N enrichment of the ML with a mean NO3 increase from 56 to 93 nM corresponding to a NO3 integrated stocks increase by $888\,\mathrm{\mu mol\,N\,m^{-2}}$ (Fig. 3, Table S2). There was also a clear difference in the mean NO3 concentrations between the ML and NDLb (93 ± 15 vs. $51 \pm 7\,\mathrm{nM}$, respectively). This is the largest NO3 difference observed during the cruise between these two layers (Fig. 4), confirming that the ML enrichment could not be attributed to inputs from below. The relaxation of the wind burst was progressive, with a continuous deepening of the ML (Table S1). The export of the atmospheric NO3 into the NDLb was highest after the rain event (FAST $+0.24$). At the end of the FAST occupation period (FAST $+3.8$) high NO3 concentrations (mean 135 nM) were measured again within the ML.

DIP concentration dynamics were different from those of NO3, with similar integrated DIP stocks within the ML being measured 6 h before and 6 h after the rain ($136\,\mathrm{\mu mol\,m^{-2}}$). From then on, DIP stocks progressively increased reaching a maximum ($281\,\mathrm{\mu mol\,P\,m^{-2}}$) 1 d after the rain (FAST $+1$).

Immediately after the rain, integrated PP (euphotic zone) decreased from $274\,\mathrm{mg\,C\,m^{-2}\,d^{-1}}$ (FAST -0.9) to $164\,\mathrm{mg\,C\,m^{-2}\,d^{-1}}$ (FAST $+0.07$) and continued to decrease the following day. It was only 3.8 d after the rain that PP returned to initial values (Table S2). Such variations were mostly due to changes in PP within the DCM depth (Fig. S2), as the values did not change significantly within the ML (28–$33\,\mathrm{mg\,C\,m^{-2}\,d^{-1}}$; Figs. S2, 5). Integrated BP in the upper 200 m of the water column showed the opposite trend to that of PP, increasing from $86 \pm 3\,\mathrm{mg\,C\,m^{-2}\,d^{-1}}$ ($n = 4$) before the rain up to $113\,\mathrm{mg\,C\,m^{-2}\,d^{-1}}$ at FAST $+0.5$ (Table S2). Although modest, this increasing trend was also visible over the ML (12–15 to 15–$19\,\mathrm{mg\,C\,m^{-2}\,d^{-1}}$ after the rain event). The abundances of picophytoplankton groups varied mostly in the vicinity of the DCM depth with peaks occurring 1–2 d after the rain (grey profiles, Fig S3), in particular for prokaryotes (*Prochlorococcus*, *Synechococcus*). Heterotrophic prokaryotes and nanoflagellate abundances increased slightly within the DCM depth after the rain.

4 Discussion

The specific context of the oceanographic survey constrained the temporal and spatial coverage of our analysis as the biogeochemical responses to a rain event were investigated over a few days (3–5) and tens of kilometers (40–50). Their evolution was restricted to the vertical dimension, integrating lateral exchanges by horizontal diffusion or local advection that occurred over the corresponding space scales and timescales. In the vertical dimension, exchanges of nutrients across the ML were controlled by mixing due to rapidly changing conditions (MLD fluctuations along with nutrient inputs from the atmosphere) rather than diffusion. Four groups of stations, corresponding to different stages of ML enrichment and relaxation, due to the nutrient inputs from single rain events, have been characterized based on the differences in NO3 concentration between the ML and NDLb (see Sect. 2.4). As shown in Fig. 4, this succession of stages is in agreement with the NO3 fluxes from above and below the ML. Moreover, they provide a temporal scaling of the oceanic response to atmospheric deposition, with a quasi-instantaneous change at the time of the rain event and a 2 d relaxation period necessary to recover pre-event conditions.

In this context, we will (i) discuss the nitrogen budget within the ML at the short stations considered a "snapshot" and (ii) analyze in detail, using a time series of CTD casts, the biogeochemical changes within the ML and the NDLb following the atmospheric wet deposition event at FAST, discussing the possible modes of transfer of nutrients between these two layers.

4.1 A snapshot of biological fluxes in the ML and their link to new DIN from atmospheric dry deposition

The dependence of hprok on nutrients rather than on labile organic carbon during stratification conditions is not uncommon in the MS (Van Wambeke et al., 2002; Céa et al., 2014; Sala et al., 2002) and has also been shown during the PEACETIME cruise (P or N–P co-limitation, Fig. S4). Hprok have an advantage due to their small cell size and their kinetic systems which are adapted to extremely low concentrations of nutrients (for example for DIP see Talarmin et al., 2015). Under such conditions of limitation, hprok will react rapidly to new phosphorus and nitrogen inputs, coming from atmospheric deposition. During an artificial in situ DIP enrichment experiment in the eastern Mediterranean, P rapidly circulated through hprok and heterotrophic ciliates, and the phytoplankton were not directly linked to this "bypass" process (Thingstad et al., 2005). Bioassays conducted in the tropical Atlantic Ocean have also shown that hprok respond more strongly than phytoplankton to nutrients from Saharan aerosols (Marañón et al., 2010), a pattern that has been confirmed in a meta-analysis of dust addition experiments (Guieu et al., 2014a; Guieu and Ridame, 2021; Gazeau et al., 2021).
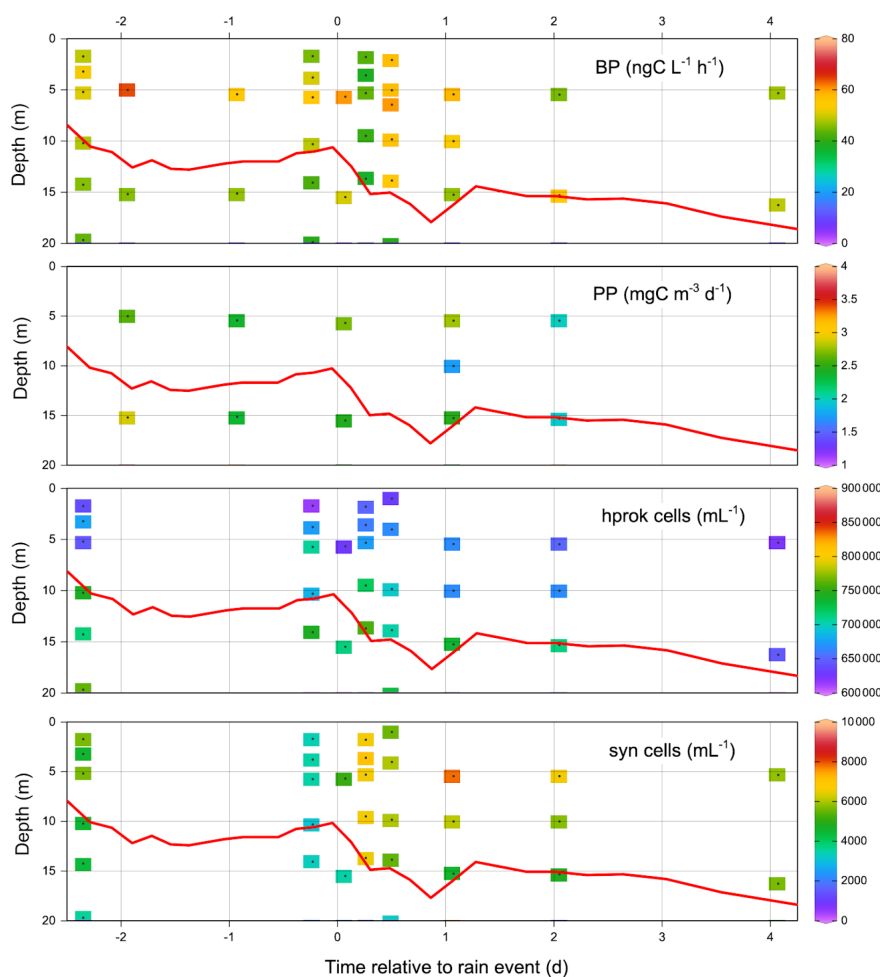
Figure 5. Evolution within the ML of heterotrophic prokaryotic production (BP), primary production (PP), heterotrophic prokaryotes (hprok) and *Synechococcus* (syn) abundances at FAST. The mixed layer depth is indicated by a red line.

We considered hprokN demand together with phytoN demand and compared it to autochthonous (DON hydrolysis by ectoenzymatic activity) and allochthonous (atmospheric deposition) sources. To the best of our knowledge this is the first time that these fluxes are compared based on their simultaneous quantification at sea. High variability was observed among the 10 short stations (Table 2). The regeneration of nitrogen through aminopeptidase activity was clearly the primary provider of N to hprok as 14 % to 66 % (mean ± SD of 37 % ± 19 %) of the hprokN demand could be satisfied by in situ LAP activity. Such percentages may be largely biased by the conversion factors from C to N and propagation of errors for the LAP hydrolysis rates and BP rates. However, the C/N ratio of hprok is relatively constant even under large variations in P or N limitation (6.2 to 8.4; Nagata, 1986).

Other regeneration sources exist such as the direct excretion of NH4 or low-molecular-weight DON sources with no necessity for hydrolysis prior to uptake (Jumars et al., 1989). For instance, Feliú et al. (2020) calculated that NH4 and DIP excretion by zooplankton would satisfy 25 %–43 % of the phytoN demand and 22 %–37 % of the phytoP demand over the whole euphotic zone. Such percentages suggest that direct excretion by zooplankton along with ectoenzymatic activity provide substantial N for biological activity.

N_2 fixation is also a source of new N that can fuel hprok directly, as some diazotrophs are heterotrophic (Delmont et al., 2018, and references therein), or indirectly, as part of the fixed N_2 that rapidly cycles through hprok (Caffin et al., 2018). Furthermore, it has been observed that there is a better coupling of N2fix rates with BP rather than with PP in the eastern MS (Rahav et al., 2013b). This was also observed within the ML in this study. Our data showed that the hypothetical contribution of N2fix to hprokN demand within the ML was low (6.4 ± 2.4 %) and consistent with the low N2fix observed in the MS (i.e., Rahav et al., 2013a; Ibello et al., 2010; Ridame et al., 2011; Bonnet et al., 2011). This differs from other parts of the ocean primarily limited by N but not by P, such as the southeastern Pacific where N2fix are high (Bonnet et al., 2017) and can represent up to 81 % of the hprokN demand (Van Wambeke et al., 2018).

The sum of LAP activity and N2fix was not sufficient to meet hprokN demand (total contribution between 19 % and 73 % of hprokN demand). We examined the importance of new DIN from dry atmospheric deposition. Atmospheric DIN fluxes from dry deposition showed a low variability along the transect ($29 \pm 7\,\mu mol\,N\,m^{-2}\,d^{-1}$ at the short stations) and were among the lowest previously measured in the Mediterranean basin, ranging from 38 to $240\,\mu mol\,N\,m^{-2}\,d^{-1}$ (Desboeufs, 2021). It has to be noted that the fluxes measured during the PEACETIME cruise are representative of the open sea atmosphere, while published fluxes were measured at coastal sites where local/regional contamination contributes significantly to the fluxes (Desboeufs, 2021). Atmospheric deposition also delivers organic matter (Djaoudi et al., 2017; Kanakidou et al., 2018), which is bioavailable for marine hprok (Djaoudi et al., 2020). Dissolved organic nitrogen (DON) released from aerosols, not determined here, can be estimated from previous studies. On average in the MS, DON solubilized from aerosols represents 32 %. (range 19 % to 42 %) of the total dissolved N released from dry deposition (Desboeufs, 2021). Considering this mean, DON released from dry deposition was estimated to range from 8 to $19\,\mu mol\,N\,m^{-2}\,d^{-1}$ at the short-duration stations. The total dissolved N solubilized from dry deposition (inorganic measured + organic estimated) would thus represent 14 % to 121 % of the hprokN demand. Because of the low variability in DIN (and estimated DON) fluxes derived from dry deposition, the atmospheric contribution was mainly driven by biogeochemical processes in the water column and not by the variability in atmospheric fluxes during the cruise (coefficient of variation of hprokN demand and phytoN demand at the short stations was 45 % and 89 %, respectively, and that of DIN flux was 25 %). However, the calculated contribution can also be biased by the deposition velocity used to calculate DIN solubilized from the dry deposition. Deposition velocity was set at $1\,cm\,s^{-1}$ for NO3 and $0.21\,cm\,s^{-1}$ for NH4. As NO3 was the dominant inorganic form released by dry deposition, it is clear that the choice of $1\,cm\,s^{-1}$ for NO3 influenced its contribution. This choice was conditioned by the predominance of NO3 in the main types of aerosols in the Mediterranean basin such as dust or sea salt particles (e.g., Bardouki et al., 2003). However, the deposition velocity of NO3 between fine and large particles could range from 0.6 to $2\,cm\,s^{-1}$ in these aerosols (e.g., Sandroni et al., 2007). Even considering the lower value of $0.6\,cm\,s^{-1}$ from the literature, the contribution of DIN from atmospheric dry deposition to hprokN demand within the ML would still be significant (up to 72 %).

4.2 Biogeochemical response after a wet deposition event – N and P budgets at FAST

Rain events are more sporadic than dry atmospheric deposition but represent much higher new nutrient fluxes to the MS surface waters on an annual basis, e.g., on average 84 % of annual atmospheric DIN fluxes on Corsica (Desboeufs et al., 2018). At the scale of the Mediterranean basin, the annual wet deposition of DIN was found to be 2–8 times higher than DIN from dry deposition (Markaki et al., 2010). Wet deposition also contributes significantly to DON atmospheric fluxes in the MS: for example at the Frioul Archipelago (Bay of Marseille, NW MS), total (wet + dry) DON atmospheric fluxes ranged between 7 and $367\,\mu mol\,DON\,m^{-2}\,d^{-1}$ and represented $41 \pm 14\,\%$ of the total atmospheric nitrogen flux (Djaoudi et al., 2018). In the eastern MS (Lampedusa) DON atmospheric fluxes ranged between 1.5 and $250\,\mu mol\,DON\,m^{-2}\,d^{-1}$, contributing 25 % of the total atmospheric nitrogen flux (Galletti et al., 2020). In both studies, bulk atmospheric fluxes of DON were positively correlated with precipitation rates, indicating the preponderance of wet over dry deposition.

At FAST, the maximum net variations in NO3 and DIP concentrations within the ML after the rainy period reached $1520 - 665 = +855\,\mu mol\,N\,m^{-2}$ for NO3 and $281 - 137 = +144\,\mu mol\,P\,m^{-2}$ for DIP (Table S2). In other terms, based on a mean MLD of 16 m, the net observed increases in the ML were +9 nM DIP and +54 nM NO3. These net variations observed in the ML are higher than the calculated variation in stocks deduced from the N and P concentrations of this rain event (0.07 nM DIP and 21 nM NO3 concentration increase over the whole ML; Table 3). This is still true when including all P or N chemical species (particulate and soluble inorganic + organic fractions) with, for example, an increase in P concentration in the ML of ~ 0.68 nM. As described in the Results, Sect. 3.4, the rains affecting the FAST site were spatially patchy over a large area (~ 40–50 km radius around the research vessel). Thus, we consider that the biogeochemical impacts observed at the FAST site were probably due to a suite of atmospheric events rather than only the single event observed on board. It is also possible that mesoscale and sub-mesoscale dynamics encountered at the FAST site (Figs. 5 and 12 in Guieu et al., 2020) may have affected such a cumulative impact.

Interestingly, a delay of about 19 h was observed in the maximum net accumulation within the ML between DIP (FAST +1.05) and NO3 (FAST +0.24). The DIN/DIP ratio in the rain (1438) was much higher than the Redfield ratio. As the biological turnover of DIP in the MS is rapid (from minutes to a few hours; Talarmin et al., 2015), new DIP from rain might have behaved differently than DIN. Two different mechanisms can explain this delay: (i) processes linked to bypasses and luxury DIP uptake (storage of surplus P in hprok before a rapid development of grazers – Flaten et al., 2005; Herut et al., 2005; Thingstad et al., 2005 – that are later responsible for DIP regeneration) so that DIP net accumulation is delayed and/or (ii) abiotic processes such as rapid desorption from large sinking particles followed by adsorption of DIP onto submicronic iron oxides still in suspension as observed experimentally in Louis et al. (2015).

The first proposed mechanism may be supported by the observed increase in BP, along with stable PP, which suggests an immediate benefit of the new nutrients from rain to hprok rather than phytoplankton. The so-called luxury DIP uptake by organisms like hprok is efficient (small cells with high surface / volume ratio and DIP kinetic uptake adapted to low concentrations). It is of course difficult to quantify such in situ variations in comparison to mesocosm/minicosm dust addition experiments, in which heterotrophy was clearly promoted (Marañón et al., 2010; Guieu et al., 2014b; Gazeau et al., 2021). A few field studies have confirmed these trends (Herut et al., 2005; Pulido-Villena et al., 2008), but, as stated in the Introduction, these studies lacked high-frequency sampling.

The second proposed mechanism, the abiotic adsorption followed by desorption, is compatible with the observed 19 h delay (Louis et al., 2015). Note that most of the estimates of such abiotic processes are from dust addition experiments with contrasting results, some showing this abiotic process of absorption followed by desorption while the particles are sinking (Louis et al., 2015) and others not (Carbo et al., 2005; Ridame et al., 2003). It is possible that DIP adsorbed onto large particles rapidly sinks out of the ML and desorbs partly during its transit in the PDLb, where it can remain for longer periods due to the stratification at the pycnoclines.

We calculated a tentative P budget between FAST $+1.05$ and FAST $+2.11$ where a net ML decrease in DIP ($-87\,\mu$mol P m^{-2}) was observed. During this time, advective flux of DIP into the PDLb was not detectable as DIP concentrations within the ML were always lower than within the PDLb (Pulido-Villena et al., 2021). This indicated that DIP was assimilated and/or transformed into DOP via biological processes and/or adsorbed onto particles and exported to PDLb by sedimentation. By integrating PP and BP over this period (34.5 and 19.7 mg C m^{-2}, respectively) and assuming that the 87 μmol DIP m^{-2} removed was consumed by hprok and phytoplankton, the C/P ratio of their biomass would be 52. Such a C/P ratio suggests that DIP was not limiting these organisms anymore. Indeed a decrease in C/P quotas may highlight a switch from P to C limitation for heterotrophic bacteria (Godwin and Cotner, 2015) and from P to N limitation or increased growth rates for phytoplankton (Moreno and Martiny, 2018). Furthermore, as DIP is also recycled via alkaline phosphatase within the ML, we also consider another source of DIP via alkaline phosphatase activity, which could release 139 μmol DIP m^{-2} during this period (see Van Wambeke et al., 2021, for in situ estimates). Assuming also that DIP resulting from AP hydrolysis was fully assimilated by the plankton, the C/P ratio would be 19. This low ratio seems unrealistic for phytoplankton (Moreno and Martigny, 2018) as well as hprok, even growing in surplus C conditions (Makino et al., 2003; Lovdal et al., 2008; Godwin and Cotner, 2015).

Some of the P recycled in or brought into the ML from atmospheric deposition has consequently been exported below the ML. DIP is abiotically adsorbed on mineral dust particles (Louis et al., 2015) and is exported out of the ML during particle sinking. It is also possible that such processes enable the export of other P-containing organic molecules, such as DOP or viruses produced following luxury DIP assimilation. Free viruses, richer in P than N relative to hprok, could adsorb, like DOM, onto dust particles and constitute a P export source. Indeed, free viruses adsorb onto black carbon particles, possibly reducing viral infection (Mari et al., 2019; Malits et al., 2015). However, particle quality is a determining factor for DOM or microbial attachment, and what has been shown for black carbon particles is not necessarily true for dust particles. For instance, the addition of Saharan dust to marine coastal waters led to a negligible sorption of viruses to particles and increased abundance of free viruses (Pulido-Villena et al., 2014), possibly linked to an enhancement of lytic cycles in the ML after relieving limitation (Pradeep Ram and Sime-Ngando, 2010).

We are aware of all the assumptions made here, including (i) conversion factors; (ii) in situ estimates of alkaline phosphatase; (iii) some missing DIP sources in the budget, such as the excretion of zooplankton estimated to amount to 22 %–37 % of the phytoP demand at the FAST site (Feliú et al., 2020); (iv) lack of knowledge on the different mechanisms linking P to dust particles; and (v) considering the station to be a 1D system. Nevertheless, all these results together suggest that both luxury consumption by hprok and export via scavenging on mineral particles probably occurred simultaneously and could explain the observed variations in DIP in the ML.

For NO3, and in contrast to the observations for DIP, we observed physical exchanges by advection between the ML and NDLb. A N budget within the ML during the period of net NO3 decrease (between FAST $+0.24$ and FAST $+2.11$, Table S2) indicates a net loss of 1343 μmol N m^{-2}. For this period lasting 1.8 d, the time-integrated phytoN and hprokN demands were 682 and 378 μmol N m^{-2}, respectively, so total biological demand in the ML was 1060 μmol N m^{-2}. During this period, the possible N sources used were NO3 which decreased by 1343 μmol N m^{-2} as well as N$_2$ fixation at 13 μmol N m^{-2} and in situ aminopeptidase activity at 87 μmol N m^{-2}. In total, these possible sources of N amounted to 1443 μmol N m^{-2}. Keeping in mind that the same potential caveats mentioned for DIP (see above) also apply to the N budget, the biological N demand appeared to be lower than the sources (difference $\sim$ 380 μmol N m^{-2}). On the other hand, at FAST, vertical advective fluxes of NO3 from the ML to NDLb were up to 337 μmol N m^{-2} d^{-1} (Fig. 4); i.e., $\sim$ 600 μmol N m^{-2} was lost from the ML over 1.8 d. From these two different approaches, exported NO3 should range between 380 and 600 μmol N m^{-2} over this period. Thus, about 40 % of the NO3 accumulated in the ML after the rain was likely exported by vertical advection to the NDLb. Organisms present in the DCM could benefit from this input of new nutrients. Indeed, PP and abundances of all
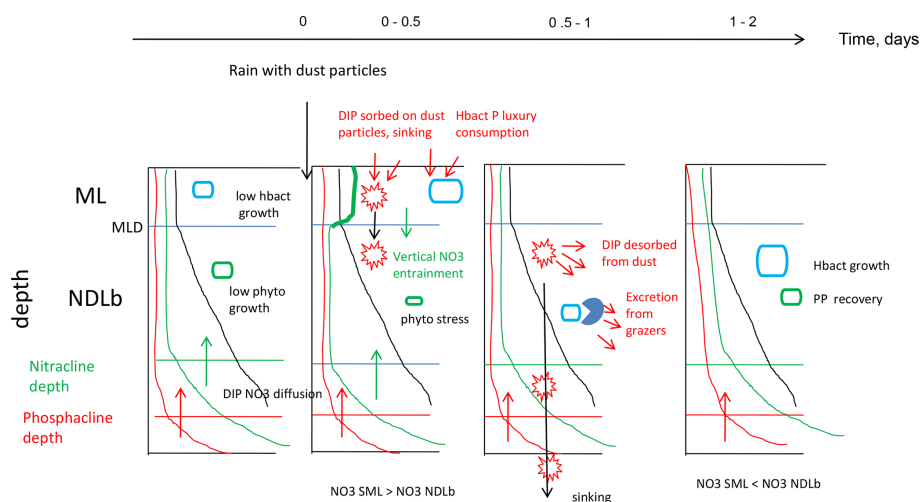
Figure 6. Synthetic view of biogeochemical processes and exchanges between the ML and NDLb at FAST before the rain and evolution after the rain.

four phytoplankton groups (*Synechococcus*, *Prochlorococcus*, nano- and picoeukaryotes) increased at the DCM after 24 h and remained high for 2 d after the rain event (Fig. S3). The increase in abundances were higher for prokaryotic phytoplankton abundances as such organisms would likely benefit from their small size and their ability to use DON/DOP from organic molecules (Yelton et al., 2016).

5 Conclusions

This study reports for the first time, in the context of an oceanographic cruise, simultaneous sampling of atmospheric and ocean biogeochemical parameters to characterize the in situ biogeochemical responses to atmospheric deposition within the ML. High-frequency sampling, in particular at FAST, confirmed the transitory state of exchanges between the ML and the NDLb. Even though dry deposition measured along the transect was homogeneous and among the lowest observed in the MS, that input could represent up to 121 % of the hprokN demand.

Our results have shown the important role played by the ML in the biogeochemical and physical processes responsible for transfers of nutrients between the atmosphere and the nutrient-depleted layer below. Thanks to the use of the LWCC technique and access to nanomolar values of NO3 and DIP in repeated CTD casts, it was possible to demonstrate the role of the ML and exchanges of NO3 from the ML to the NDLb by vertical advection when variations in MLD occurred simultaneously with transitory accumulation of NO3 after a deposition event. The time sequence occurring after a wet dust deposition event was summarized as follows (Fig. 6): accumulation of NO3 in the ML; advection to the NDLb; luxury consumption of DIP by hprok and delayed peaks of DIP; and decrease in primary production and

subsequent recovery after 2 d, mainly visible in the nutrient-depleted layer. Dust deposition triggers a complex and time-controlled trophic cascade within the microbial food web. Our study shows the important role of intermittent but strong abiotic effects such as downwelling advective fluxes from the ML to the nutrient-depleted layers. It will be important to consider these aspects in biogeochemical budgets and models, especially as climate and anthropogenic changes are predicted to increase aerosol deposition in the Mediterranean Sea.

Author contributions. CG and KD designed the study. FVW measured ectoenzymatic activity, and BP and AE managed the TAA analysis and treatments; EPV measured DIP with the LWCC technique; CR measured nitrogen fixation; VT assisted in CTD operations and analyzed water masses; JD sampled for dissolved organic carbon and flow cytometry; EM analyzed the primary production data; FVW prepared the manuscript with contributions from all co-authors.

References

Aminot, A. and Kérouel, R.: Dosage automatique des nutriments dans les eaux marines, in: Méthodes d'analyses en milieu marin, edited by: IFREMER, MEDD, Éditions Quae, Plouzané, France, 188 pp., IBSN 978-2-7592-0023-8, 2007.

Bardouki, H., Liakakou, H., Economou, C., Sciare, J., Smolik, J., Zdimal, V., Eleftheriadis, K., Lazaridis, M., Dye, C., and Mihalopoulos, N.: Chemical composition of size resolved atmospheric aerosols in the eastern Mediterranean during summer and winter, Atmos. Environ., 37, 195–208, 2003.

Bonnet, S., Grosso, O., and Moutin, T.: Planktonic dinitrogen fixation along a longitudinal gradient across the Mediterranean Sea during the stratified period (BOUM cruise), Biogeosciences, 8, 2257–2267, https://doi.org/10.5194/bg-8-2257-2011, 2011.

Bonnet, S., Caffin, M., Berthelot, H., and Moutin, T.: Hot spot of N_2 fixation in the western tropical South Pacific pleads for a spatial decoupling between N_2 fixation and denitrification, PNAS letter, 144, E2800–E2801, https://doi.org/10.1073/pnas.1619514114, 2017.

Caffin, M., Berthelot, H., Cornet-Barthaux, V., Barani, A., and Bonnet, S.: Transfer of diazotroph-derived nitrogen to the planktonic food web across gradients of N_2 fixation activity and diversity in the western tropical South Pacific Ocean, Biogeosciences, 15, 3795–3810, https://doi.org/10.5194/bg-15-3795-2018, 2018.

Carbo, P., Krom, M. D., Homoky, W. B., Benning, L. G., and Herut, B.: Impact of atmospheric deposition on N and P geochemistry in the southeastern Levantine basin, Deep-Sea Res. Pt. II, 52, 3041–3053, https://doi.org/10.1016/j.dsr2.2005.08.014, 2005.

Céa, B., Lefèvre, D., Chirurgien, L., Raimbault, P., Garcia, N., Charrière, B., Grégori, G., Ghiglione, J.-F., Barani, A., Lafont, M., and Van Wambeke, F.: An annual survey of bacterial production, respiration and ectoenzyme activity in coastal NW Mediterranean waters: temperature and resource controls, Environ. Sci. Pollut. Res., 22, 13654–13668, https://doi.org/10.1007/s11356-014-3500-9, 2014.

Christaki, U., Courties, C., Massana, R., Catala, P., Lebaron, P., Gasol, J. M., and Zubkov, M.: Optimized routine flow cytometric enumeration of heterotrophic flagellates using SYBR Green I, Limnol. Oceanogr. Methods, 9, 329–339, https://doi.org/10.4319/lom.2011.9.329, 2011.

Cullen, J. J., Franks, P. J., Karl, D. M., and Longhurst, A. L. A. N.: Physical influences on marine ecosystem dynamics, The sea, 12, 297–336, 2002.

de Boyer Montegut, C., Madec, G., Fisher, A. S., Lazar, A., and Iudicone, D.: Mixed layer depth over the global ocean: An examination of profile data and a profile-based climatology, J. Geophys. Res.-Oceans, 109, C12003, https://doi.org/10.1029/2004JC002378, 2004.

Delmont, T. O., Quince, C., Shaiber, A., Esen, Ö. C., Lee, S. T. M., Rappé, M. R., McLellan, S. L., Lücker, S., and Murat Eren, A.: Nitrogen-fixing populations of Planctomycetes and Proteobacteria are abundant in surface ocean metagenomes, Nat. Microbiol., 3, 804–813, https://doi.org/10.1038/s41564-018-0176-9, 2018.

Desboeufs, K.: Nutrients atmospheric deposition and variability, in: Atmospheric Chemistry and its Impacts in the Mediterranean Region, volume 2 – From Air pollutants Sources to Impacts, edited by: Dulac, F., Sauvage, S., and Hanoumou, E., Springer, Switzerland, eBook ISBN 978-3-030-82385-6, Chapter 16, in press, available at: https://www.springer.com/gp/book/9783030823849 last access: 20 October 2021.

Desboeufs, K., Bon Nguyen, E., Chevaillier, S., Triquet, S., and Dulac, F.: Fluxes and sources of nutrient and trace metal atmospheric deposition in the northwestern Mediterranean, Atmos. Chem. Phys., 18, 14477–14492, https://doi.org/10.5194/acp-18-14477-2018, 2018.

Desboeufs, K., Fu, F., Bressac, M., Tovar-Sánchez, A., Triquet, S., Doussin, J.-F., Giorio, C., Chazette, P., Disnaquet, J., Feron, A.,

Formenti, P., Maisonneuve, F., Rodrí´guez-Romero, A., Zapf, P., Dulac, F., and Guieu, C.: Wet deposition in the remote western and central Mediterranean as a source of trace metals to surface seawater, Atmos. Chem. Phys. Discuss. [preprint], https://doi.org/10.5194/acp-2021-624, in review, 2021.

Dittmar, T. H., Cherrier, J., and Ludwichowski, K.-U.: The analysis of amino acids in seawater, in: Practical Guidelines for the Analysis of Seawater, edited by: Wurl, O., Boca Raton, FL, CRC-Press, 67–78, 2009.

Djaoudi, K., Van Wambeke, F., Barani, A., Hélias-Nunige, S., Sempéré, R., and Pulido-Villena, E.: Atmospheric fluxes of soluble organic C, N, and P to the Mediterranean Sea: potential biogeochemical implications in the surface layer, Prog. Oceanogr., 163, 59–69, MERMEX special issue, https://doi.org/10.1016/j.pocean.2017.07.008, 2017.

Djaoudi, K., Van Wambeke, F., Coppola, L., D'ortenzio, F., Helias-Nunige, S., Raimbault, P., Taillandier, V., Testor, P., Wagener, T., and Pulido-Villena, E.: Sensitive determination of the dissolved phosphate pool for an improved resolution of its vertical variability in the surface layer: New views in the P-depleted Mediterranean Sea, Frontiers in Marine Science, 5, 234, https://doi.org/10.3389/fmars.2018.00234, 2018.

Djaoudi, K., Van Wambeke, F., Barani, A., Bhairy, N., Chevaillier, S., Desboeufs, K., Nunige, S., Labiadh, M., Henry des Tureaux, T., Lefèvre, D., Nouara, A., Panagiotopoulos, C., Tedetti, M., and Pulido-Villena, E.: Potential bioavailability of organic matter from atmospheric particles to marine heterotrophic bacteria, Biogeosciences, 17, 6271–6285, https://doi.org/10.5194/bg-17-6271-2020, 2020.

D'Ortenzio, F., Iudicone, D., de Boyer Montegut, C., Testor, P., Antoine, D., Marullo, S., Santoleri, R., and Madec, G.: Seasonal variability of the mixed layer depth in the Mediterranean Sea as derived from in situ profiles, Geophys. Res. Lett., 32, L12605, https://doi.org/10.1029/2005GL022463, 2005.

Du, C., Liu, Z., Kao, S.-J., and Dai, M.: Diapycnal fluxes of nutrients in an oligotrophic oceanic regime: The South China Sea, Geophys. Res. Lett., 44, 11510–11518, https://doi.org/10.1002/2017GL074921, 2017.

Feliú, G., Pagano, M., Hidalgo, P., and Carlotti, F.: Structure and function of epipelagic mesozooplankton and their response to dust deposition events during the spring PEACETIME cruise in the Mediterranean Sea, Biogeosciences, 17, 5417–5441, https://doi.org/10.5194/bg-17-5417-2020, 2020.

Flaten, G. A., Skjoldal, E. F., Krom, M. D., Law, C. S., Mantoura, F. C., Pitta, P., Psarra, S., Tanaka, T., Tselepides, A., Woodward, E. M., Zohary, T., and Thingstad, T. F.: Studies of the microbial P-cycle during a Lagrangian phosphate-addition experiment in the Eastern Mediterranean, Deep-Sea Res. Pt. II, 52, 2928–2943, 2005.

Galletti, Y., Becagli, S., di Sarra, A., Gonnelli, M., Pulido-Villena, E., Sferlazzo, D. M., Traversi, R., Vestri, S., and Santinelli, C.: Atmospheric deposition of organic matter at a remote site in the central Mediterranean Sea: implications for the marine ecosystem, Biogeosciences, 17, 3669–3684, https://doi.org/10.5194/bg-17-3669-2020, 2020.

Gasol, J. M. and del Giorgio, P. A.: Using flow cytometry for counting natural planktonic bacteria and understanding the structure of planktonic bacterial communities, Sci. Mar., 64, 197–224, 2000.

Gazeau, F., Van Wambeke, F., Marañón, E., Pérez-Lorenzo, M., Alliouane, S., Stolpe, C., Blasco, T., Leblond, N., Zäncker, B., Engel, A., Marie, B., Dinasquet, J., and Guieu, C.: Impact of dust addition on the metabolism of Mediterranean plankton communities and carbon export under present and future conditions of pH and temperature, Biogeosciences, 18, 5423–5446, https://doi.org/10.5194/bg-18-5423-2021, 2021.

Godwin, C. M. and Cotner, J. B.: Aquatic heterotrophic bacteria have highly flexible phosphorus content and biomass stoichiometry, the ISME Journal, 9, 2324–2327, https://doi.org/10.1038/ismej.2015.34, 2015.

Guieu, C., and Ridame, C.: Impact of atmospheric deposition on marine chemistry and biogeochemistry, in: Atmospheric Chemistry in the Mediterranean Region, volume 2 – From Air pollutants Sources to Impacts, edited by: Dulac, F., Sauvage, S., and Hanoumou, E., Springer, Switzerland, eBook IBSN 978-3-030-82385-6, Chapter 22, https://www.springer.com/gp/book/9783030823849, last access: 20 October 2021.

Guieu, C., Dulac, F., Desboeufs, K., Wagener, T., Pulido-Villena, E., Grisoni, J.-M., Louis, F., Ridame, C., Blain, S., Brunet, C., Bon Nguyen, E., Tran, S., Labiadh, M., and Dominici, J.-M.: Large clean mesocosms and simulated dust deposition: a new methodology to investigate responses of marine oligotrophic ecosystems to atmospheric inputs, Biogeosciences, 7, 2765–2784, https://doi.org/10.5194/bg-7-2765-2010, 2010.

Guieu, C., Aumont, O., Paytan, A., Bopp, L., Law, C. S., Mahowald, N., Achterberg, E. P., Marañón, E., Salihoglu, B., Crise, A., Wagener, T., Herut, B., Desboeufs, K., Kanakidou, M., Olgun, N., Peters, F., Pulido-Villena, E., Tovar-Sanchez, A., and Völker, C.: The significance of episodicity in atmospheric deposition to Low Nutrient Low Chlorophyll regions, Global Biogeochem. Cy., 28, 1179–1198, https://doi.org/10.1002/2014GB004852, 2014a.

Guieu, C., Ridame, C., Pulido-Villena, E., Bressac, M., Desboeufs, K., and Dulac, F.: Impact of dust deposition on carbon budget: a tentative assessment from a mesocosm approach, Biogeosciences, 11, 5621–5635, https://doi.org/10.5194/bg-11-5621-2014, 2014b.

Guieu, C., Desboeufs, K., Albani, S., Alliouane, S., Aumont, O., Barbieux, M., Barrillon, S., Baudoux, A.-C., Berline, L., Bhairy, N., Bigeard, E., Bloss, M., Bressac, M., Brito, J., Carlotti, F., de Liege, G., Dinasquet, J., Djaoudi, K., Doglioli, A., D'Ortenzio, F., Doussin, J.-F., Duforet, L., Dulac, F., Dutay, J.-C., Engel, A., Feliu-Brito, G., Ferre, H., Formenti, P., Fu, F., Garcia, D., Garel, M., Gazeau, F., Giorio, C., Gregori, G., Grisoni, J.-M., Guasco, S., Guittonneau, J., Haëntjens, N., Heimburger, L.-E., Helias, S., Jacquet, S., Laurent, B., Leblond, N., Lefevre, D., Mallet, M., Marañón, E., Nabat, P., Nicosia, A., Obernosterer, I., Perez, L. M., Petrenko, A., Pulido-Villena, E., Raimbault, P., Ridame, C., Riffault, V., Rougier, G., Rousselet, L., Roy-Barman, M., Saiz-Lopez, A., Schmechtig, C., Sellegri, K., Siour, G., Taillandier, V., Tamburini, C., Thyssen, M., Tovar-Sanchez, A., Triquet, S., Uitz, J., Van Wambeke, F., Wagener, T., and Zaencker, B.: BIOGEOCHEMICAL dataset collected during the PEACETIME cruise, SEANOE [data set], https://doi.org/10.17882/75747, 2020.

Guieu, C., D'Ortenzio, F., Dulac, F., Taillandier, V., Doglioli, A., Petrenko, A., Barrillon, S., Mallet, M., Nabat, P., and Desboeufs, K.: Introduction: Process studies at the air–sea interface after atmospheric deposition in the Mediterranean Sea – objectives and strategy of the PEACETIME oceanographic

campaign (May–June 2017), Biogeosciences, 17, 5563–5585, https://doi.org/10.5194/bg-17-5563-2020, 2020.

Heimburger, A., Losno, R., Triquet, S., Dulac F., and Mahowald, N. M.: Direct measurements of atmospheric iron, cobalt and aluminium-derived dust deposition at Kerguelen Islands, Global Biogeochem. Cy., 26, GB4016, https://doi.org/10.1029/2012GB004301, 2012.

Hersbach, H., Bell, B., Berrisford, P., Biavati, G., Horányi, A., Muñoz Sabater, J., Nicolas, J., Peubey, C., Radu, R., Rozum, I., Schepers, D., Simmons, A., Soci, C., Dee, D., and Thépaut, J.-N.: ERA5 hourly data on single levels from 1979 to present, Copernicus Climate Change Service (C3S) Climate Data Store (CDS), https://doi.org/10.24381/cds.adbb2d47, 2018.

Herut, B., Zohary, T., Krom, M. D., Mantoura, R. F. C., Pitta, P., Psarra, S., Rassoulzadegan, F., Tanaka, T., and Thingstad, T. F.: Response of East Mediterranean surface water to Saharan dust: On-board microcosm experiment and field observations, Deep-Sea Res. Pt. II, 52, 3024–3040, 2005.

Herut, B., Rahav, E., Tsagaraki, T. M., Giannakourou, A., Tsiola, A., Psarra, S., Lagaria, A., Papageorgiou, N., Mihalopoulos, N., Theodosi, C. N., Violaki, K., Stathopoulou, E., Scoullos, M., Krom, M. D., Stockdale, A., Shi, Z., Berman-Frank, I., Meador, T. B., Tanaka, T., and Paraskevi, P.: The potential impact of Saharan dust and polluted aerosols on microbial populations in the East Mediterranean Sea, an overview of a mesocosm experimental approach, Front. Mar. Sci, 3, 226, https://doi.org/10.3389/fmars.2016.00226, 2016.

Hoppe, H.-G., Ducklow, H., and Karrasch, B.: Evidence for dependency of bacterial growth on enzymatic hydrolysis of particulate organic matter in the mesopelagic ocean, Mar. Ecol. Prog. Ser., 93, 277–283, 1993.

Ibello, V., Cantoni, C., Cozzi, S., and Civitarese, G.: First basin-wide experimental results on N2 fixation in the open Mediterranean Sea, Geophys. Res. Lett., 37, L03608, https://doi.org/10.1029/2009GL041635, 2010.

Izquierdo, R., Benítez-Nelson, C. R., Masqué, P., Castillo, S., Alastuey, A., and Àvila, A.: Atmospheric phosphorus deposition in a near-coastal rural site in the NE Iberian Peninsula and its role in marine productivity, Atmos. Environ., 49, 361–370, https://doi.org/10.1016/j.atmosenv.2011.11.007, 2012.

Jumars, P. A., Penry, D. L., Baross, J. A., Perry, M. A., and Frost, B. W.: Closing the microbial loop: dissolved carbon pathway to heterotrophic bacteria from incomplete ingestion, digestion and absorption in animals, Deep-Sea Res., 483–495, 1989.

Kamykowski, D. and Zentara, S. J.: Nitrate and silicic acid in the world ocean: Patterns and processes, Mar. Ecol. Prog. Ser., 26, 47–59, 1985.

Kanakidou, M., Myriokefalitakis, S., and Tsigaridis, K.: Aerosols in atmospheric chemistry and biogeochemical cycles of nutrients, Environ. Res. Lett., 13, 063004, https://doi.org/10.1088/1748-9326/aabcdb, 2018.

Kanakidou, M., Myriokefalitakis, S., and Tsagkaraki, M.: Atmospheric inputs of nutrients to the Mediterranean Sea, Deep-Sea Res.-Pt. I, 171, 104606, https://doi.org/10.1016/j.dsr2.2019.06.014, 2020.

Kirchman, D. L.: Leucine incorporation as a measure of biomass production by heterotrophic bacteria, in: Handbook of methods in aquatic microbial ecology, edited by: Kemp, P. F., Sherr, B. F., Sherr, E. B., and Cole, J. J.,

Lewis, Boca Raton, 509–512, eBook ISBN 978-0-203-75274-6, https://doi.org/10.1201/9780203752746, 1993.

Kouvarakis, G., Mihalopoulos, N., Tselepides, T., and Stavrakakis, S.: On the importance of atmospheric nitrogen inputs on the productivity of eastern Mediterranean, Global Biogeochem. Cycles, 15, 805–818, https://doi.org/10.1029/2001GB001399, 2001.

Krom, M. D., Herut, B., and Mantoura, R. F. C.: Nutrient budget for the eastern Mediterranean: Implication for phosphorus limitation, Limnol. Oceanogr., 49, 1582–1592, https://doi.org/10.4319/lo.2004.49.5.1582, 2004.

Louis, J., Bressac, M., Pedrotti, M.-L., and Guieu, C.: Dissolved inorganic nitrogen and phosphorus dynamics in sea water following an artificial Saharan dust deposition event, Frontiers in Marine Science, 2, 27, https://doi.org/10.3389/fmars.2015.00027, 2015.

Løvdal, T., Skjoldal, E. F., Heldal, M., Norland, S., and Thingstad, T. F.: Changes in Morphology and Elemental Composition of Vibrio splendidus Along a Gradient from Carbon-limited to Phosphate-limited Growth, Microb. Ecol., 55, 152–161, https://doi.org/10.1007/s00248-007-9262-x, 2008.

Makino, W., Cotner, J. B., Sterner, R. W., and Elser, J. J.: Are bacteria more like plants or animals? Growth rate and resource dependence of bacterial C : N : P stoichiometry, Funct. Ecol., 17, 121–130, 2003.

Malits, A., Cattaneo, R., Sintes, E., Gasol, J. M., Herndl, G. J., and Weinbauer, M.: Potential impacts of black carbon on the marine microbial community, Aquat. Microb. Ecol., 75, 27–42, https://doi.org/10.3354/ame01742, 2015.

Marañón, E., Fernández, A., Mouriño-Carballido, B., Martínez-García, S., Teira, E., Cermeño, P., Chouciño, P., Huete-Ortega, M., Fernández, E., Calvo-Díaz, A., Morán, X. A. G., Bode, A., Moreno-Ostos, E., Varela, M. M., Patey, M. D., and Achterberg, E. P.: Degree of oligotrophy controls the response of microbial plankton to Saharan dust, Limnol. Oceanogr., 55, 2339–2352, 2010.

Marañón, E., Van Wambeke, F., Uitz, J., Boss, E. S., Dimier, C., Dinasquet, J., Engel, A., Haëntjens, N., Pérez-Lorenzo, M., Taillandier, V., and Zäncker, B.: Deep maxima of phytoplankton biomass, primary production and bacterial production in the Mediterranean Sea, Biogeosciences, 18, 1749–1767, https://doi.org/10.5194/bg-18-1749-2021, 2021.

Mari, X., Guinot, B., Chu, V. T., Brune, J., Lefebvre, J.-P., Pradeep Ram, A. S., Raimbault, P., Dittmar, T., and Niggemann, J.: Biogeochemical Impacts of a Black Carbon Wet Deposition Event in Halong Bay, Vietnam, Frontiers in Marine Science, 6, 185, https://doi.org/10.3389/fmars.2019.00185, 2019.

Marie, D., Simon, N., Guillou, L., Partensky, F., and Vaulot, D.: Flow Cytometry Analysis of Marine Picoplankton, in: In Living Color: Protocols in Flow Cytometry and Cell Sorting, edited by: Diamond, R. A. and Demaggio, S., Springer, Berlin, Heidelberg, 421–454, eBook ISBN 978-3-642-57049-0, 2000.

Markaki, Z., Loye-Pilot, M. D., Violaki, K., Benyahya, L., and Mihalopoulos, N.: Variability of atmospheric deposition of dissolved nitrogen and phosphorus in the Mediterranean and possible link to the anomalous seawater N/P ratio, Mar. Chem., 120, 187–194, https://doi.org/10.1016/j.marchem.2008.10.005, 2010.

Martiny, A. C., Pham, C. T. A., Primeau, F. W., Vrugt, J. A., Moore, J. K., Levin, S. A., and Lomas, M. W.: Strong latitudinal patterns in the elemental ratios of marine plankton and organic mat-

ter, Nat. Geosci., 6, 279–283, https://doi.org/10.1038/ngeo1757, 2013.

MERMEX Group: Marine ecosystems' responses to climatic and anthropogenic forcings in the Mediterranean, Prog. Oceanogr., 91, 97–166, https://doi.org/10.1016/j.pocean.2011.02.003, 2011.

Mescioglu, E., Rahav, E., Frada, M. J., Rosenfeld, S., Raveh, O., Galletti, Y., Santinelli, C., Herut, B., and Paytan, A.: Dust-associated airborne microbes affect primary and bacterial production rates, and eukaryote diversity, in the Northern Red Sea: A mesocosm approach, Atmosphere, 10, 358, https://doi.org/10.3390/atmos10070358, 2019.

Moreno, A. R. and Martiny, A. C.: Ecological stoichiometry of ocean plankton, Ann. Rev. Mar. Sci., 10, 43–69, 2018.

Nagata, T.: Carbon and Nitrogen content of natural planktonic bacteria, Appl. Environ. Microbiol., 52, 28–32, 1986.

Omand, M. M. and Mahadevan, A.: The shape of the oceanic nitracline, Biogeosciences, 12, 3273–3287, https://doi.org/10.5194/bg-12-3273-2015, 2015.

Orsini, D., Ma, Y., Sullivan, A., Sierau, B., Baumann, K., and Weber, R.: Refinements to the Particle-Into-Liquid Sampler (PILS) for Ground and Airborne Measurements of Water Soluble Aerosol Composition, Atmos. Environ., 37, 1243–1259, 2003.

Pradeep Ram, A. S. and Sime-Ngando, T.: Resources drive trade-off between viral lifestyles in the plankton: evidence from freshwater microbial microcosms, Environ. Microbiol., 12, 467–479, https://doi.org/10.1111/j.1462-2920.2009.02088.x, 2010.

Prieur, L., D'Ortenzio, F., Taillandier, V., and Testor, P.: Physical oceanography of the Ligurian sea, in: the Mediterranean sea in the era of global change (volume 1), evidence from 30 years of multidisciplinary study of the Ligurian sea, edited by: Migon, C., Sciandra, A., and Nival, P., ISTE Sci. Publ. LTD, 49–78, https://doi.org/10.1002/9781119706960.ch3, 2020.

Pujo-Pay, M. and Raimbault, P.: Improvements of the wet-oxidation procedure for simultaneous determination of particulate organic nitrogen and phosphorus collected on filters, Mar. Ecol. Prog. Ser., 105, 203–207, 1994.

Pulido-Villena, E., Wagener, T., and Guieu, C.: Bacterial response to dust pulses in the western Mediterranean: Implications for carbon cycling in the oligotrophic ocean, Global Biogeochem. Cy., 22, GB1020, https://doi.org/10.1029/2007GB003091, 2008.

Pulido-Villena, E., Rérolle, V., and Guieu, C.: Transient fertilizing effect of dust in P-deficient surface LNLC ocean, Geophys. Res. Lett., 37, L01603, https://doi.org/10.1029/2009GL041415, 2010.

Pulido-Villena, E., Baudoux, A.-C., Obernosterer, I., Landa, M., Caparros, J., Catala, P., Georges, C., Harmand, J., and Guieu, C.: Microbial food web dynamics in response to a Saharan dust event: results from a mesocosm study in the oligotrophic Mediterranean Sea, Biogeosciences, 11, 5607–5619, https://doi.org/10.5194/bg-11-5607-2014, 2014.

Pulido-Villena, E., Desboeufs, K., Djaoudi, K., Van Wambeke, F., Barrillon, S., Doglioli, A., Petrenko, A., Taillandier, V., Fu, F., Gaillard, T., Guasco, S., Nunige, S., Triquet, S., and Guieu, C.: Phosphorus cycling in the upper waters of the Mediterranean Sea (Peacetime cruise): relative contribution of external and internal sources, Biogeosciences Discuss. [preprint], https://doi.org/10.5194/bg-2021-94, in review, 2021.

Rahav, E., Herut, B., Levi, A., Mulholland, M. R., and Berman-Frank, I.: Springtime contribution of dinitrogen fixation to pri-

mary production across the Mediterranean Sea, Ocean Sci., 9, 489–498, https://doi.org/10.5194/os-9-489-2013, 2013a.

Rahav, E., Herut, B., Stambler, N., Bar-Zeev, E. Mulholland, M. R., and Berman-Frank, I.: Uncoupling between dinitrogen fixation and primary productivity in the eastern Mediterranean Sea, J. Geophys. Res.-Biogeosci., 118, 195–202, https://doi.org/10.1002/jgrg.20023, 2013b.

Rahav, E., Paytan, A., Chien, C.-T., Ovadia, G., Katz, T., and Herut, B.: The Impact of Atmospheric Dry Deposition Associated Microbes on the Southeastern Mediterranean Sea Surface Water following an Intense Dust Storm, Frontiers in Marine Science, 3, 127, https://doi.org/10.3389/fmars.2016.00127, 2016.

Richon, C., Dutay, J. C., Dulac, F., Wang, R., Balkanski, Y., Nabat, P., Aumont, O., Desboeufs, K., Laurent, B., Guieu, C., Raimbault, P., and Beuvier, J.: Modeling the impacts of atmospheric deposition of nitrogen and desert dust-derived phosphorus on nutrients and biological budgets of the Mediterranean Sea, Prog. Oceanogr, 163, 21–39, https://doi.org/10.1016/j.pocean.2017.04.009, 2018.

Ridame, C., Moutin, T., and Guieu, C.: Does phosphate adsorption onto Saharan dust explain the unusual N/P ratio in the Mediterranean Sea?, Oceanol. Acta, 26, 629–634, https://doi.org/10.1016/S0399-1784(03)00061-6, 2003.

Ridame, C., Le Moal, M., Guieu, C., Ternon, E., Biegala, I. C., L'Helguen, S., and Pujo-Pay, M.: Nutrient control of N_2 fixation in the oligotrophic Mediterranean Sea and the impact of Saharan dust events, Biogeosciences, 8, 2773–2783, https://doi.org/10.5194/bg-8-2773-2011, 2011.

Sala, M. M., Peters, F., Gasol, J. M., Pedros-Alio, C., Marrasse, C., and Vaque, D.: Seasonal and spatial variations in the nutrient limitation of bacterioplankton growth in the northwestern Mediterranean, Aquat. Microb. Ecol., 27, 47–56, 2002.

Sandroni, V., Raimbault, P., Migon, C., Garcia, N., and Gouze, E.: Dry atmospheric deposition and diazotrophy as sources of new nitrogen to northwestern Mediterranean oligotrophic surface waters, Deep-Sea Res. Pt. I, 54, 1859–1870, https://doi.org/10.1016/j.dsr.2007.08.004, 2007.

Schlitzer, R.: Ocean Data View, [code], available at: https://odv.awi.de, last access: 13 October 2021.

Taillandier, V., Prieur, L., D'Ortenzio, F., Ribera d'Alcalà, M., and Pulido-Villena, E.: Profiling float observation of thermohaline staircases in the western Mediterranean Sea and impact on nutrient fluxes, Biogeosciences, 17, 3343–3366, https://doi.org/10.5194/bg-17-3343-2020, 2020.

Talarmin, A., Van Wambeke, F., Lebaron, P., and Moutin, T.: Vertical partitioning of phosphate uptake among picoplankton groups in the low Pi Mediterranean Sea, Biogeosciences, 12, 1237–1247, https://doi.org/10.5194/bg-12-1237-2015, 2015.

Tanaka, T., Thingstad, T. F., Christaki, U., Colombet, J., Cornet-Barthaux, V., Courties, C., Grattepanche, J.-D., Lagaria, A., Nedoma, J., Oriol, L., Psarra, S., Pujo-Pay, M., and Van Wambeke, F.: Lack of P-limitation of phytoplankton and heterotrophic prokaryotes in surface waters of three anticyclonic eddies in the stratified Mediterranean Sea, Biogeosciences, 8, 525–538, https://doi.org/10.5194/bg-8-525-2011, 2011.

Thingstad, T., Krom, M. D., Mantoura, F., Flaten, G., Groom, S., Herut, B., Kress, N., Law, C. S., Pasternak, A., Pitta, P., Psarra, S., Rassoulzadegan, F., Tanaka, T., Tselepides, A., Wassmann, P., Woodward, M., Riser, C., Zodiatis, G., and

Zohary, T.: Nature of phosphorus limitation in the ultra-oligotrophic eastern Mediterranean, Science, 309, 1068–1071, https://doi.org/10.1126/science.1112632, 2005.

Tovar-Sánchez, A., Rodríguez-Romero, A., Engel, A., Zäncker, B., Fu, F., Marañón, E., Pérez-Lorenzo, M., Bressac, M., Wagener, T., Triquet, S., Siour, G., Desboeufs, K., and Guieu, C.: Characterizing the surface microlayer in the Mediterranean Sea: trace metal concentrations and microbial plankton abundance, Biogeosciences, 17, 2349–2364, https://doi.org/10.5194/bg-17-2349-2020, 2020.

Van Wambeke, F., Christaki, U., Giannakourou, A., Moutin, T., and Souvemerzoglou, K.: Longitudinal and vertical trends of bacterial limitation by phosphorus and carbon in the Mediterranean Sea, Microb. Ecol., 43, 119–133, https://doi.org/10.1007/s00248-001-0038-4, 2002.

Van Wambeke, F., Gimenez, A., Duhamel, S., Dupouy, C., Lefevre, D., Pujo-Pay, M., and Moutin, T.: Dynamics and controls of heterotrophic prokaryotic production in the western tropical South Pacific Ocean: links with diazotrophic and photosynthetic activity, Biogeosciences, 15, 2669–2689, https://doi.org/10.5194/bg-15-2669-2018, 2018.

Van Wambeke, F., Pulido, E., Catala, P., Dinasquet, J., Djaoudi, K., Engel, A., Garel, M., Guasco, S., Marie, B., Nunige, S., Taillandier, V., Zäncker, B., and Tamburini, C.: Spatial patterns of ectoenzymatic kinetics in relation to biogeochemical properties in the Mediterranean Sea and the concentration of the fluorogenic substrate used, Biogeosciences, 18, 2301–2323, https://doi.org/10.5194/bg-18-2301-2021, 2021.

Yelton, A. P., Acinas, S. G., Sunagawa, S., Bork, P., Pedros-Alio, C., and Chisholm, S. W.: Global genetic capacity for mixotrophy in marine picocyanobacteria, ISME J., 10, 2946–2957, 2016.

Zhang, J.-Z. and Chi, J.: Automated analysis of nano-molar concentrations of phosphate in natural waters with liquid waveguide, Environ. Sci. Technol., 36, 1048–1053, https://doi.org/10.1021/es011094v, 2002.